A Blueprint of Sex-Specific Neuronal Regulation in *the C. elegans* Nervous System at Single-Cell Resolution

Rizwanul Haque[1,2,*], Hagar Setty[1,2,*], Ramiro Lorenzo[3,*], Gil Stelzer[4], Ron Rotkopf[4], Yehuda Salzberg[1,2], Gal Goldman[1], Sandeep Kumar[5], Shiraz Nir Halber[1,2], Andrew M. Leifer[5,6], Elad Schneidman[1], Patrick Laurent[3] and Meital Oren-Suissa[1,2]

[1]Department of Brain Sciences, Weizmann Institute of Science, Rehovot 76100, Israel

[2]Department of Molecular Neuroscience, Weizmann Institute of Science, Rehovot, Israel

[3]Laboratory of Neurophysiology, ULB Neuroscience Institute (UNI), Université Libre de Bruxelles (ULB), Brussels, Belgium

[4]Bioinformatics Unit- Life Science Core Facilities, Weizmann Institute of Science, Israel

[5]Princeton Neuroscience Institute, Princeton University, Princeton, NJ 08544, USA

[6]Department of Physics, Princeton University, Princeton, NJ 08544, USA

*Equal contribution

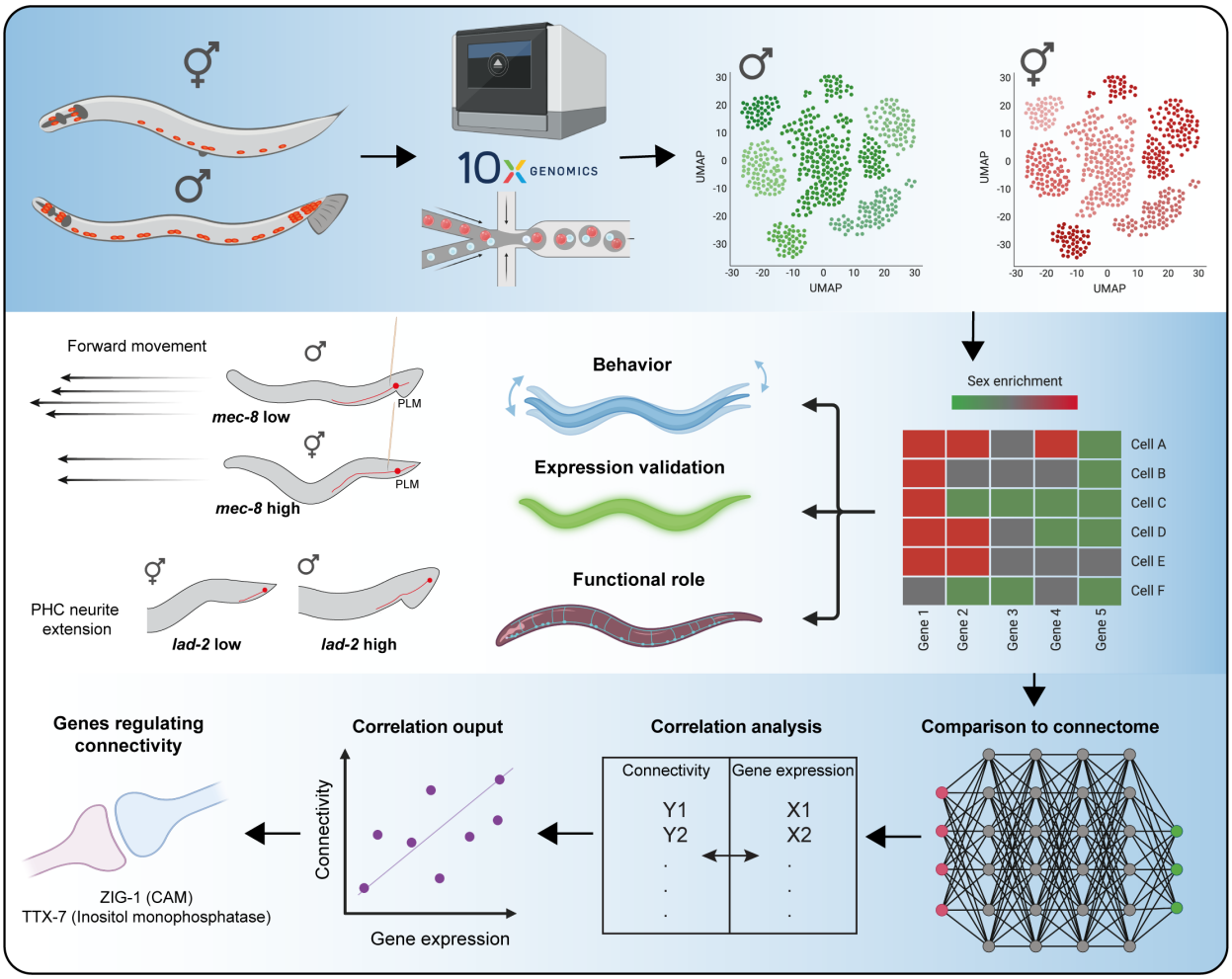
10X GENOMICS
UMAP
UMAP
UMAP
UMAP
Forward movement
mec-8 low
PLM
mec-8 high
PLM
PHC neurite extension
lad-2 low
lad-2 high
Behavior
Expression validation
Functional role
Sex enrichment
Cell A
Cell B
Cell C
Cell D
Cell E
Cell F
Gene 1
Gene 2
Gene 3
Gene 4
Gene 5
Comparison to connectome
Correlation analysis
Connectivity
Gene expression
Y1
Y2
X1
X2
Correlation ouput
Connectivity
Gene expression
Genes regulating connectivity
ZIG-1 (CAM)
TTX-7 (Inositol monophosphatase)

ABSTRACT

Sex-specific behaviors within a species are often attributed to variances in neuronal wiring and molecular signatures. However, how the genetic sex shapes the molecular architecture of the nervous system at a single neuron level is still unknown. To address this gap, we used single-cell RNA-sequencing (scRNA-seq) to profile the transcriptome of the sex-shared nervous system of adult male and hermaphrodite *Caenorhabditis elegans*. By ranking neurons based on the degree of molecular dimorphism, we uncover novel sexually dimorphic neurons such as PLM neurons, where functional dimorphism was corroborated by diminished posterior touch responses in hermaphrodites. We identify sex-specific regulators of mechanosensory behavior and neuronal function by combining our dataset with reverse genetic screens. While most sex-shared neurons retain their neurotransmitter identity, the male neuropeptide connectome undergoes substantial remodeling, with most of the neuropeptides showing a male-bias expression. This reinforces the notion that neuropeptides are crucial for diversifying connectome outputs. Furthermore, by correlating gene expression with outgoing synaptic connectivity, we identified regulatory candidates for synaptic wiring, including both shared and sex-specific genes. This comprehensive resource provides foundational insights into the molecular drivers of sexual dimorphism, facilitating future exploration of regulatory mechanisms and their impact on sex-specific behaviors in higher organisms.

38 **INTRODUCTION**

39 The molecular mechanisms that underlie the development of sex differences in the nervous
40 system have been the focus of many studies in the past decade, especially due to the sex bias
41 demonstrated in the prevalence and progression of several neurological diseases such as anxiety
42 and Parkinson's disease[1–3]. Recent studies have made an effort to dissect sexually dimorphic
43 neuronal circuits, uncovering unique circuits across the animal kingdom that operate differently
44 between the sexes to drive behavior (termed "sexually dimorphic"); such as the circuit for
45 empathic behaviors in mice, aggressive behaviors in fruit flies and nociceptive and
46 mechanosensory behaviors in worms[4–7]. While these studies have managed to provide insights
47 into how the nervous system is differentially shaped at the level of specific circuits, a complete
48 picture of the molecular repertoire of the entire nervous system in both sexes is still lacking. With
49 the advancement of RNA sequencing, molecular profiles of both sexes in mice were generated,
50 discovering differentially expressed genes between the sexes in specific neuronal populations
51 such as the medial amygdala (MeA) and the ventromedial nucleus of the hypothalamus (VMH)[8–
52 11]. Additional studies performed transcriptomic profiling of different brain regions while
53 delineating the effect of circulating hormones on sex differences in gene expression[12–14]. Although
54 these studies provided insights regarding sexually dimorphic behaviors, they did not explore the
55 contribution of specific genes to mediate these behaviors. Additionally, the hormonal regulation
56 in mammalian systems might mask the direct effect of sexual identity (the chromosome
57 complement) on distinct molecular signatures at the level of single neurons.

58 In the nematode *Caenorhabditis elegans* (*C. elegans*), the genetic sex of each somatic cell,
59 including neurons, is determined in a cell-autonomous manner: the ratio of sex-chromosomes to

60 autosomes controls a transcriptional cascade which results in the expression of either
61 hermaphrodite-specific or male-specific genes[15,16]. Recent studies explored the contribution of
62 the genetic sex to nervous system development, with insights into synaptic connectivity, circuitry,
63 function, and behavior[7,17–19]. Despite all these efforts, we still lack a complete picture of how
64 genetic sex shapes gene expression patterns across the nervous system and the different neuronal
65 classes.
66 Recently, single-cell RNA sequencing (scRNA-seq) approaches resolved the molecular
67 heterogeneity of the hermaphrodite nervous system. Its 302 neurons were subdivided into 128
68 transcriptionally distinct neuron types[20]. The transcriptomic signatures of each neuron class
69 facilitated the identification of markers, unraveled mechanisms of cell specification, and enabled
70 deeper characterization of nervous system development and aging[20–29]. Earlier scRNA-seq
71 focused only on hermaphrodites (with one exception for glia[30]), limiting our knowledge of the
72 molecular signatures of male neurons and, most importantly, the differences in molecular
73 signatures between the sexes. To gain a broad perspective on the molecular landscape of the
74 nervous system in both sexes of *C. elegans*, we generated comparative scRNA-seq transcriptomic
75 profiles for the sex-shared neuron types in males and hermaphrodites
76 (https://www.weizmann.ac.il/dimorgena/).
77 Our research provides a comprehensive atlas for expression patterns of 18,975 genes in the
78 nervous system of adult males and hermaphrodites. This atlas revealed a variety of neuronal
79 gene classes with unique dimorphic gene expression patterns, with most of the neuropeptide-
80 encoding genes demonstrating robust sexually dimorphic gene expression. We focused on the
81 core, sex-shared nervous system i.e., neurons that exist in both sexes, and uncovered several sex-

82 shared neurons with novel dimorphic transcriptomic profiles, including the sensory touch
83 receptor neuron PLM. We harnessed our dataset to predict genes that might regulate
84 connectivity and revealed novel candidates that operate in both sexes and in a sex-specific
85 manner to control synaptic wiring.

86 **RESULTS**

87 **Single-cell sequencing of adult hermaphrodite and male nervous system**

88 To generate a single-cell transcriptomic profile of the nervous system in both sexes of *C. elegans*
89 we dissociated young adult males and hermaphrodites expressing TagRFP pan-neuronally into
90 single cells (Supplementary Figure 1A). To generate pure male populations (XO animals), we used
91 our recently published protocol that enables large-scale isolation of males with high purity[31]. To
92 isolate the fluorescently labeled neurons, we dissociated young adult animals into single cells and
93 sorted the single-cell suspensions by Fluorescence-Activated-Cell-Sorting (FACS) (Figure 1A,
94 Supplementary Figure 1B-C, *See Methods*). We confirmed the neuronal enrichment and the intact
95 morphology of RFP+ FACS-purified cells (Supplementary Figure 1D-G, *See Methods*). Single-cell
96 RNA sequencing was done using a microfluidic-based 10x genomics platform. We corrected for
97 ambient RNA, removed low-quality and damaged cells, and performed cell-quality filtering (*See*
98 *Methods*). This yielded a median of 925 unique molecular identifiers (UMIs) and 358 genes per
99 cell after filtering. To filter neurons from non-neuronal cells, we used a cutoff based on known
100 molecular landmarks (563 neuronal and 114 non-neuronal genes, Supplemental Table 1). After
101 the removal of cells containing more than 20% of UMIs originating from mitochondrial genes, we
102 obtained 13015 single-cell transcriptomes for hermaphrodites and 19454 single-cell
103 transcriptomes for males, taken for further analysis and cluster annotation.

104 To simplify cluster annotation, we merged our datasets with the previously annotated CenGEN
105 dataset[20]. This combined dataset was first segregated into 72 partitions (Supplementary Figure
106 2A). Sub-clustering of partition 1 (41219 cells) and partitions 2-72 (61546 cells) yielded 118
107 clusters (Supplementary Figure 2B-C). A further iteration included manual assignment of varying
108 identities, producing an overall of 156 clusters (details in Methods). 16 clusters were only present
109 in males and 13 were classified as "unknown ID" due to lack of previous data. We annotated
110 clusters using previously assigned cell identities[20] and manually assigned neuronal identities to
111 88 sex-shared clusters (with at least 5 cells per cluster in both sexes, Figure 1B-C). Despite the
112 underrepresentation of some neuron classes (e.g., ASH and PHB) due to limitations of cell sorting,
113 62.7% of the 118 anatomically defined neuron classes in the mature hermaphrodite nervous
114 system were captured. Interestingly, UMAP representations of sex-shared clusters of
115 hermaphrodites (adult and L4[20]) and adult males showed a large overlap (Figure 1C), with a strong
116 Spearman correlation (adult and L4, Supplementary Figure 3). When comparing UMAPs of
117 hermaphrodites (YA vs L4), we observed a subtle shift likely corresponding to the difference in
118 their developmental stage[31]. This analysis provides a framework for studying sexual dimorphism
119 in nervous system function.

120 **Single-cell profiles of the nervous system capture dimorphic gene expression**

121 In this work, we focused on the sex-shared clusters, and we did not further cluster the male-
122 specific neurons (Supplementary Table 2). For gene expression analysis, we calculated the fraction
123 of cells expressing a gene in each cluster, the average expression, and markers by using Seurat v2
124 with default parameters (*See Methods*, https://www.weizmann.ac.il/dimorgena/, Supplementary
125 Table 2). We also calculated expression thresholds as previously described ([20], *See Methods*) and

126 combined this information with the marker analysis. Predictive expression patterns across all
127 neurons in adult males and hermaphrodites can be mined using one of four thresholds of
128 increased stringency, as observed in Supplementary Table 2 (Figure 1D-E)**.** We characterized the
129 expression of genes with a known sex-biased expression. The Zn finger transcription factor LIN-
130 29 promotes a fate switch from a glutamatergic (hermaphrodite) to a cholinergic (male) identity
131 in the AIM neuron[32,33] (Figure 1F). Indeed, AIM cell clusters showed expression of *lin-29*, the
132 Choline Acetyltransferase *cho-1*/CHOT, and the vesicular Ach transporter *unc-17/VACHT* in male
133 clusters, while hermaphrodite clusters expressed the vesicular glutamate transporter *eat-*
134 *4/VGLUT* (Figure 1G). We also observed sex-biased expression of *ins-39* in male AFD neurons and
135 of *mab-3* in male SMD neurons, as previously reported (Figure 1H-I)[31,32,34].

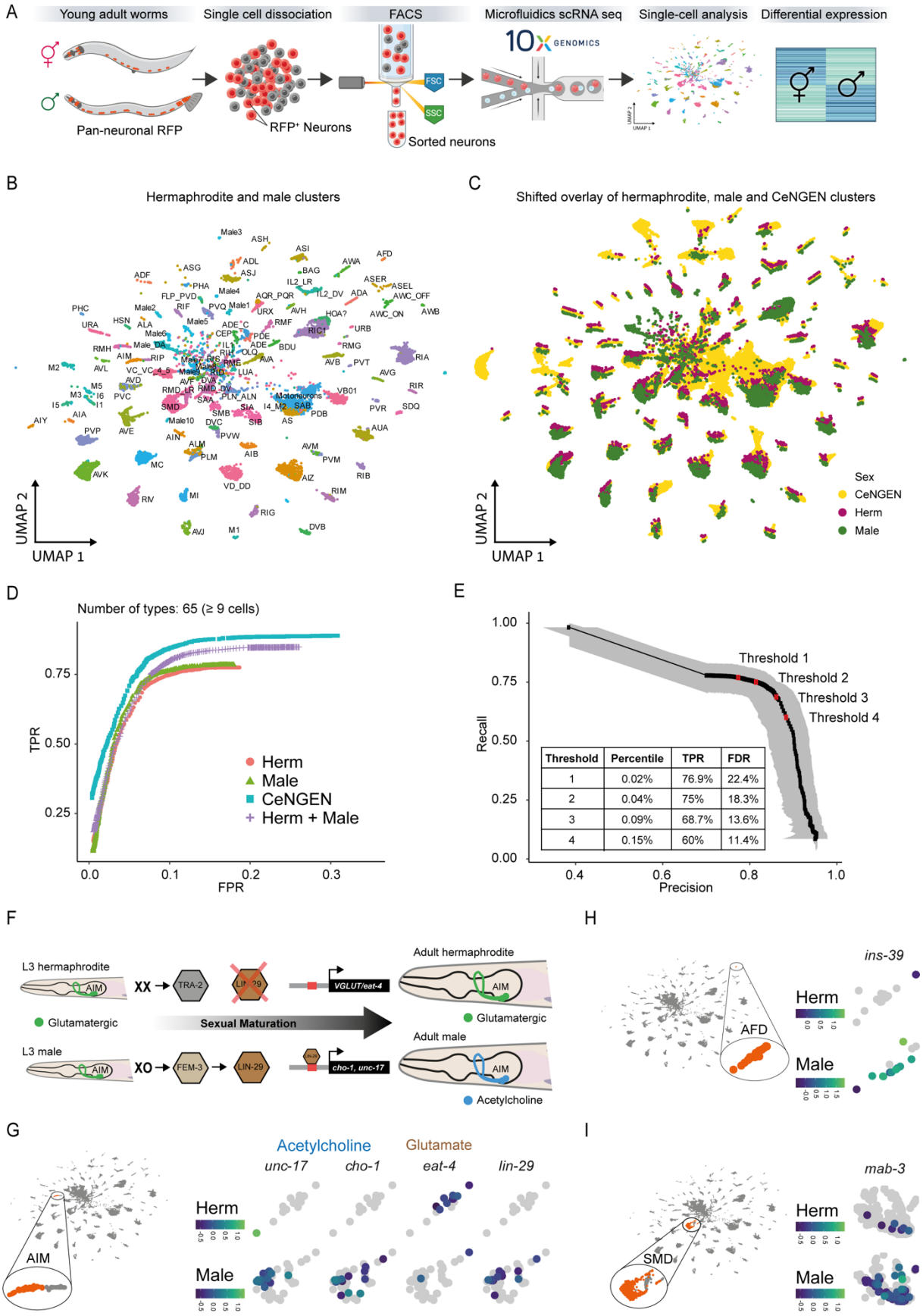
A
Young adult worms
Single cell dissociation
FACS
Microfluidics scRNA seq
Single-cell analysis
Differential expression
Pan-neuronal RFP
RFP+ Neurons
FSC
SSC
Sorted neurons
10X GENOMICS
B
Hermaphrodite and male clusters
UMAP 2
UMAP 1
C
Shifted overlay of hermaphrodite, male and CeNGEN clusters
Sex
CeNGEN
Herm
Male
D
Number of types: 65 (≥ 9 cells)
TPR
FPR
Herm
Male
CeNGEN
Herm + Male
E
Recall
Precision
Threshold 1
Threshold 2
Threshold 3
Threshold 4
Threshold | Percentile | TPR | FDR
1 | 0.02% | 76.9% | 22.4%
2 | 0.04% | 75% | 18.3%
3 | 0.09% | 68.7% | 13.6%
4 | 0.15% | 60% | 11.4%
F
L3 hermaphrodite
XX
TRA-2
LIN-29
VGLUT/eat-4
Adult hermaphrodite
AIM
Glutamatergic
Sexual Maturation
L3 male
XO
FEM-3
LIN-29
cho-1, unc-17
Adult male
Acetylcholine
H
ins-39
AFD
Herm
Male
G
Acetylcholine
Glutamate
unc-17
cho-1
eat-4
lin-29
AIM
Herm
Male
I
mab-3
SMD
Herm
Male

137 **Figure 1: Single-cell RNA sequencing in both sexes of *C. elegans***. (A) Schematic of experimental
138 design used in this study. Hermaphrodite and male *C. elegans* harboring the pan-neuronal marker
139 *rab-3p(prom1)::2xNLS::TagRFP* were subjected to cell dissociation. To purify RFP+ cells, the cell
140 suspension obtained was sorted by FACS. The single-cell RNA transcriptomes were obtained using
141 single-cell droplet microfluidic technologies (10X Genomics, https://www.10xgenomics.com). (B)
142 UMAP representation of all cell-clusters identified with their neuronal identity. Previously
143 published[20] (CenGEN) datasets or manual assignments were both used to determine the IDs of
144 the neurons. (C) UMAP representation of cell clusters with a shifted overlay to illustrate the
145 overlap. Data sets are YA hermaphrodites (magenta), YA males (green), and CenGEN L4
146 hermaphrodites (yellow). (D) Receiver-Operator Characteristic (ROC) curve showing True Positive
147 Rate (TPR) versus False Positive Rate (FPR) for hermaphrodites, males, hermaphrodites-males
148 together, and CenGEN compared to ground truth expression data using the 65 cell types with 9
149 or more cells in hermaphrodite and male clusters. (E) Precision-Recall (PR) Curve of Recall (TPR)
150 versus Precision [1 – False Discovery Rate (FDR)] curve. Red dots represent thresholds 1-4. Grey
151 shading represents 95% confidence intervals. (F) Schematic of AIM neurons neurotransmitter
152 switch from glutamatergic identity (in hermaphrodite) to cholinergic identity (in male). (G) AIM
153 representation in the UMAP projection of all cells (inset marked as orange). UMAP projection
154 depicting expression of *unc-17*, *cho-1* cholinergic identity genes, *eat-4* glutamatergic identity
155 gene, and transcriptional factor *lin-29* gene within AIM cluster. Heatmap represents expression
156 levels. (H) High expression of *ins-39* in males. AFD representation in the UMAP projection of all
157 cells (inset marked as orange). UMAP projection depicting expression of *ins-39* gene within AFD
158 cluster. Heatmap represents expression level. (I) Dimorphic expression of *mab-3*. Left, SMD
159 representation in the UMAP projection of all cells (inset marked as orange). UMAP projection
160 depicting expression of *mab-3* gene within SMD cluster. Heatmap represents expression level.
161

162 **Comparative analysis of sex-shared neuronal clusters reveals novel dimorphisms**

163 To uncover to what extent the transcriptomic profiles of the sex-shared nervous system diverge
164 between males and hermaphrodites, we took a comparative approach, ranking the sex-shared
165 neuronal clusters according to the number of differentially expressed genes (DEGs) (*See*
166 *Methods*). For ranking purposes, we filtered out clusters with more than one identity, used a
167 stricter cut-off of 9 cells per cluster in both sexes, and proceeded with 62 sex-shared clusters (*See*
168 *Methods*). This analysis captured known dimorphic sex-shared neurons, including PHC, AFD, AIM,

169 and AVG[17,32–35] (Figure 2A). Strikingly, it also revealed many sex-shared neurons that were not
170 previously classified as dimorphic, such as the six touch-receptor-neurons (TRNs), BDU, and PVR
171 interneurons (Figure 2A).
172 Gene ontology (GO) enrichment analysis for the 2216 DEGs revealed a significant proportion of
173 enriched terms related to neuronal function, suggesting their potential relevance to neuronal
174 activities (Figure 2B). Additional GO terms such as synaptic function, heteromeric G protein, and
175 calcium signaling underscore the representation of genes that may play a role in shaping a
176 dimorphic nervous system (Figure 2B). By exploring neuronal DEGs based on their gene family,
177 we found that while multiple gene families differ between the sexes, neuropeptides,
178 neuropeptide receptors, and neuropeptide metabolism-related genes are overrepresented with
179 a significant male-biased expression of neuropeptides and neuropeptides metabolism-related
180 genes (58.5%, 92 of the 157 neuropeptide genes are DEGs) (Figure 2C-D, Figure 3A,
181 Supplementary Figure 5A-B).
182 We validated the predicted sexual dimorphism in the expression pattern of two broadly expressed
183 neuropeptide genes: *nlp-11* and *flp-20,* focusing on clusters within the head or tail regions. *nlp-*
184 *11* showed dimorphic expression in 12 out of 16 predicted sex-shared neurons and in several
185 male-specific neurons (Figure 3B-F, Supplementary Figure 4A-B). The remaining four neurons
186 were either located in the midbody or difficult to identify. Similarly, *flp-20* showed sexually
187 dimorphic expression in four sex-shared neurons and in the male-specific CEMs (Supplementary
188 Figure 4C-G). Taken together, we discovered novel sexually dimorphic neurons exhibiting sex
189 differences in gene expression of various gene families, with significant prominence for the

neuropeptide family, suggesting that the peptidergic system is regulated in a highly sex-specific manner.

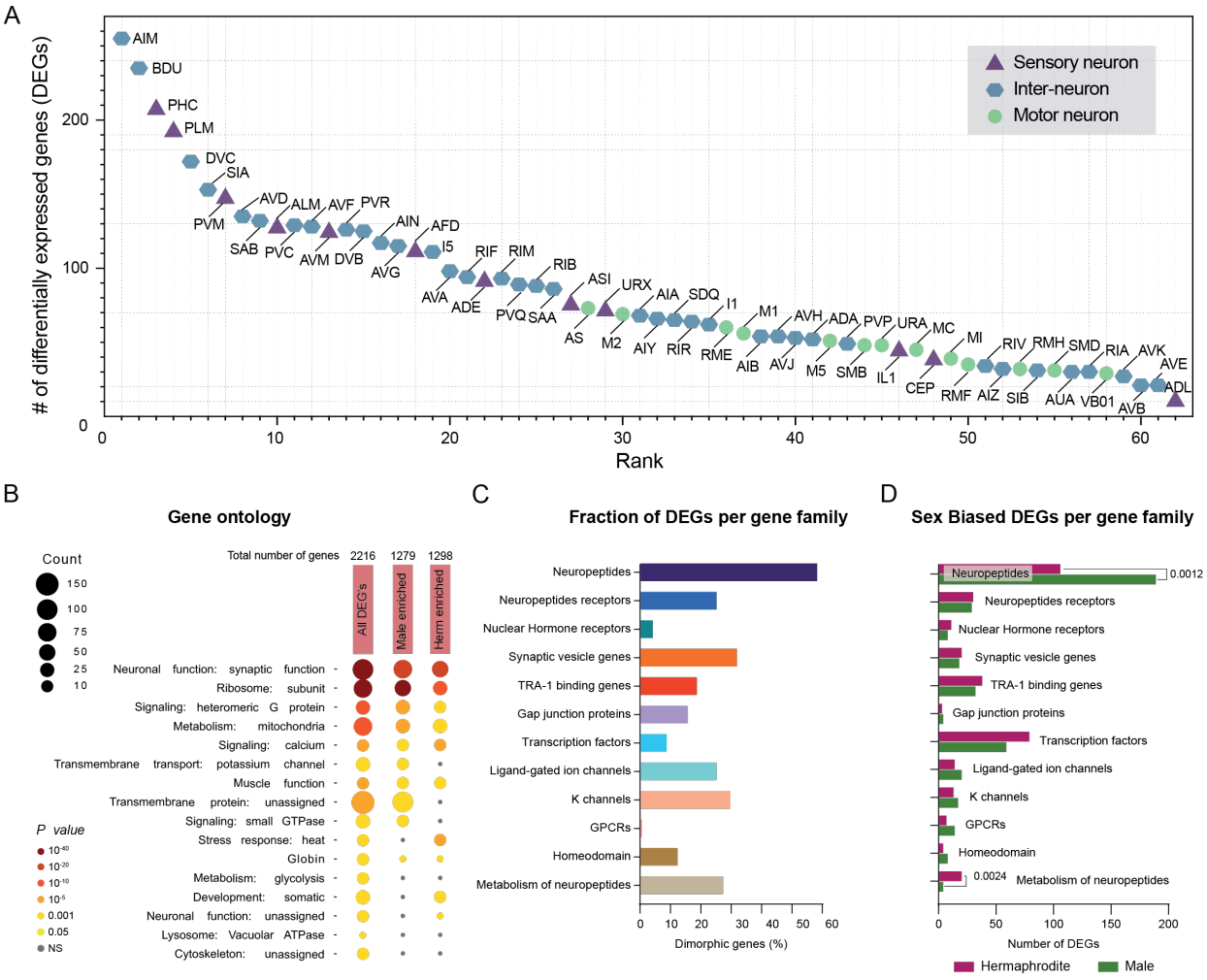

Figure 2. Ranking of sex-shared neuronal clusters highlights novel sexually dimorphic neurons. (A) The number of differentially expressed genes (DEGs) in the sex-shared neuronal clusters. Clusters are divided to sensory (triangle), interneuron (hexagon), and motor (circle) neurons. A gene was considered as DE according to the following criteria: average log fold change > 1, number of cells in a cluster ≥ 9 in both sexes, p-value < 0.05, and a threshold > 2 in at least one of the sexes (*See Methods*). (B) Gene ontology (GO) term analysis for the 2216 DEGs in both sexes and in hermaphrodite and males separately (only genes meeting the criteria of log fold change > 1, number of cells in a cluster ≥ 9 in both sexes, p-value < 0.05, threshold ≥ 2 in at least one of the sexes are included) reveals specific enrichment for synaptic and signaling gene expression. Wormcat p-values are determined by one-sided Fisher test with FDR correction. (C) Percentage of DEGs from each gene family as a fraction of the number of genes in the specific family. (D) The number of DEGs in the gene families presented in (C) divided according to DEGs that are enriched in males (green) and hermaphrodites (magenta). A DEG that is observed in more than one cluster

was counted accordingly (*See Methods*). For (D) we performed a two-sided Fisher's exact test followed by p-value Bonferroni correction for multiple comparisons.

A variety of neuronal gene families are differentially expressed between the sexes

In addition to the neuropeptide gene family, other gene families could point towards sex differences in neuronal function (Supplementary Figure 5-6). Synaptic-related genes and ion channels included only a limited number of DEGs (Figure 2C, Supplementary Figure 5C-I). Several transcription factors (TFs) are cell-specifically differentially expressed between the sexes (Supplementary Figure 6). TFs known to drive sex-specific maturation, such as *tra-1* and *mab-3,* were differentially expressed in only a few neurons (Supplementary Figure 6A-B) suggesting they may be expressed only transiently at the transition between L4 and adulthood. The TF *tbx-32* was differentially expressed in the largest number of clusters with a male bias, suggesting a previously uncharacterized role for this gene in the development of the male nervous system (Supplementary Figure 6A). DEGs also included TFs that are predicted to be bound by TRA-1 [15,36,37], supporting possible multiple unexplored roles for TFs in sex-specific neuronal regulation (Supplementary Figure 6B).

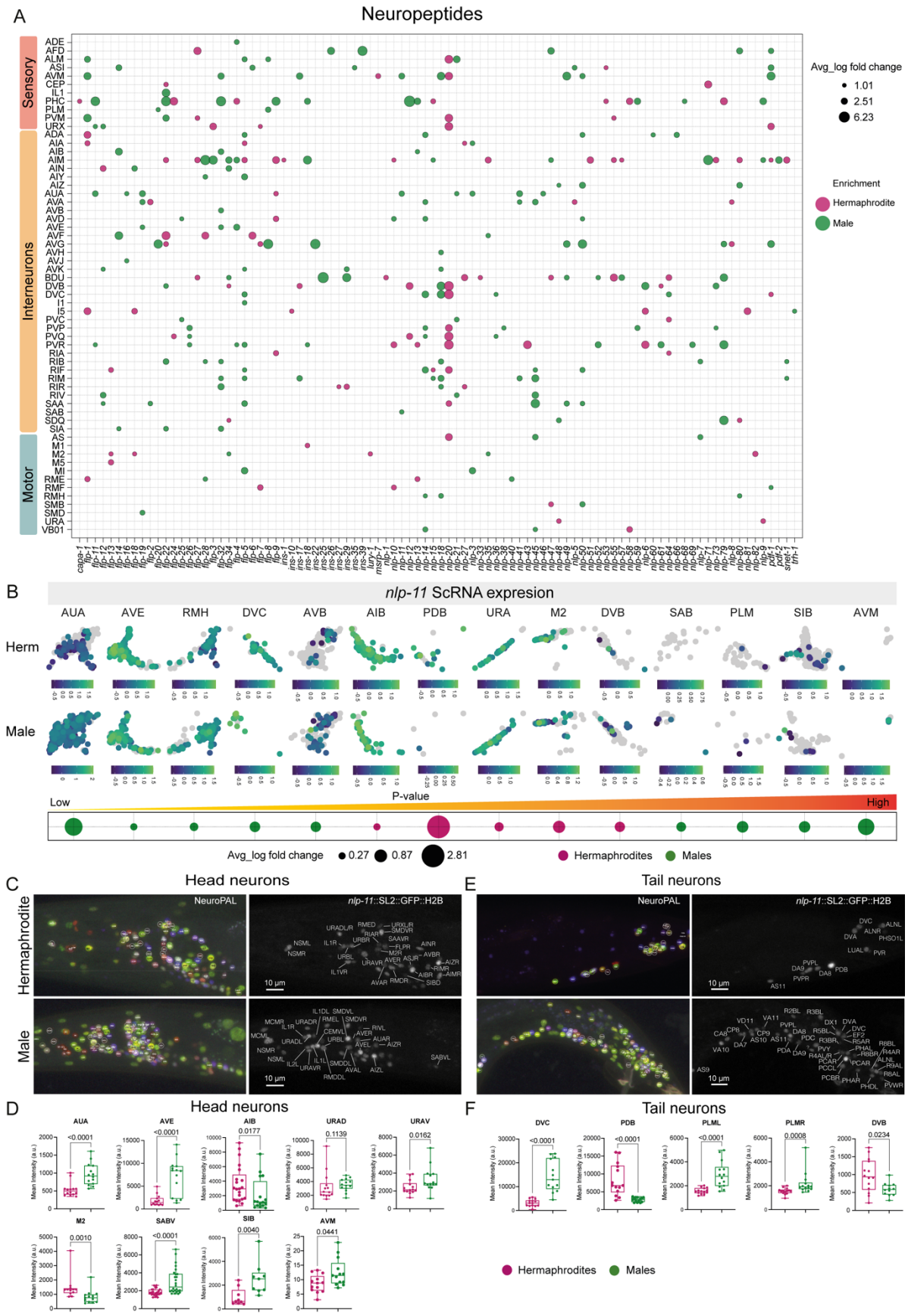
A
Neuropeptides
Sensory
Interneurons
Motor
Avg_log fold change
1.01
2.51
6.23
Enrichment
Hermaphrodite
Male
B
nlp-11 ScRNA expresion
AUA
AVE
RMH
DVC
AVB
AIB
PDB
URA
M2
DVB
SAB
PLM
SIB
AVM
Herm
Male
Low
P-value
High
Avg_log fold change
0.27
0.87
2.81
Hermaphrodites
Males
C
Head neurons
Hermaphrodite
Male
NeuroPAL
nlp-11::SL2::GFP::H2B
10 µm
E
Tail neurons
D
Head neurons
F
Tail neurons
Mean Intensity (a.u.)
Hermaphrodites
Males

Figure 3. Sexual dimorphism of neuropeptides across the nervous system. (A) Bubble plot of differentially expressed neuropeptide genes between the sexes. Bubble size corresponds to the average fold change in gene expression (only genes meeting the criteria of log fold change > 1, number of cells in a cluster ≥ 9, p-value < 0.05, threshold > 2 in at least one of the sexes are included), and bubble color indicates enrichment in either sex (green for male enrichment, magenta for hermaphrodite enrichment). Rows represent neuron types, grouped by sensory neurons, interneurons, and motor neurons. Columns represent individual genes. (B) UMAP projection of AUA, AVE, RMH, DVC, AVB, AIB, PDB, URA, M2, DVB, SAB, PLM, SIB and AVM clusters showing expression of *nlp-11* gene in both sexes. Heatmap represents the expression levels. Bubble plot representation of *nlp-11* gene expression in AUA, AVE, RMH, DVC, AVB, AIB, PDB, URA, M2, DVB, SAB, PLM, SIB and AVM clusters of the two sexes, ranked from lowest to highest p-value. Bubble size represents average log fold change, bubble color (green for males and magenta for hermaphrodites) represents enrichment in each sex. (C, E) Representative confocal micrographs showing the distinctive multi-colored neuronal nuclei in the NeuroPAL strain otIs669 in the head (C) and tail (E), a strain in which every neuron class can be uniquely identified based on its colour-based barcode[38,39]. These images were utilized to identify neurons expressing the *nlp-11(syb4759[nlp-11::SL2::GFP::H2B])* reporter in young adult hermaphrodites and males. Scale bars represent 10µm. (D) Quantification of *nlp-11* fluorescent intensity from (C) in head neurons AUA, AVE, AIB URAD, URAV, M2, SABV, SIB AVM. (F) Quantification of *nlp-11* fluorescent intensity from (E) in tail neurons DVC, PDB, PLML, PLMR, and DVB neurons in both sexes at YA stage. For each neuron group comparison, n represents the number of animals in each group in which neurons were identified and recorded. AUA, n = 14, 14 ; AVE, n = 14, 14; AIB, n = 12, 12: URAD, n = 14, 14 : URAV, n = 14, 14; M2, n = 12, 13; SABV, n = 13, 13; SIB, n = 9, 9; AVM, n = 13, 13; PDB, n = 14, 14; PLML, n = 14, 14; PLMR, n = 14, 14; DVB, n = 14, 12; DVC, n = 14, 13, for hermaphrodite and males, respectively. In the box-and-whiskers graph, the center line in the box denotes the median, while the box contains the 25th to 75th percentiles of the dataset, whiskers define the minimum and maximum value with dots showing all points. We performed a two-sided Mann-Whitney test for each comparison.

Neurotransmitter identities are mostly maintained in sex-shared neurons

Among the unique functional features that define neuron types are the neurotransmitters they use[33,40–43]. Since our analysis revealed numerous sex-shared neurons with a sexually dimorphic gene expression profile, we wondered whether these neurons maintained their neurotransmitter identity across the sexes. For this purpose, we examined the expression of neurotransmitter-related genes in hermaphrodite and male sex-shared neuronal clusters (same clusters shown Figure 2A, Figure 4A). While the known AIM neurotransmitter switch is fully captured in our data set (Figure 1F-G, Figure 4A), we did not observe any other similar cases in the other sex-shared

260 neurons (Figure 4A). However, when examining the differential expression of these
261 neurotransmitter-related genes, we found that some of them, mostly cholinergic-related and
262 glutamatergic-related genes, exhibited biased expression in several sex-shared clusters (Figure
263 4B), suggesting sexual dimorphism may be more prominent in neurotransmitter release rather
264 than identity.

265 With this in mind, we explored the relationship between dimorphic neurotransmitter release and
266 dimorphic synaptic connectivity. The complete synaptic wiring diagram of the nervous system is
267 available in *C. elegans* for both sexes[35], enabling a comparison of the number of synaptic
268 connections to neurotransmitter-related DEGs. We hypothesized that neurons that show higher
269 expression of neurotransmitter-related genes in one sex, might also have more outgoing
270 connections. To test this, we correlated the difference in connectivity between the sexes in
271 outgoing, incoming, and all synaptic connections (chemical connections)[35] (Figure 4C*, See*
272 *Methods*) with the average log-fold change of neurotransmitter-related genes presented in Figure
273 4B. Strikingly, Pearson correlation coefficient was significant only for outgoing connections but
274 not for incoming or all synaptic connections (Figure 4D). These results indicate that to some
275 extent, neurotransmitter release of a neuron is correlated with its outgoing connectivity.

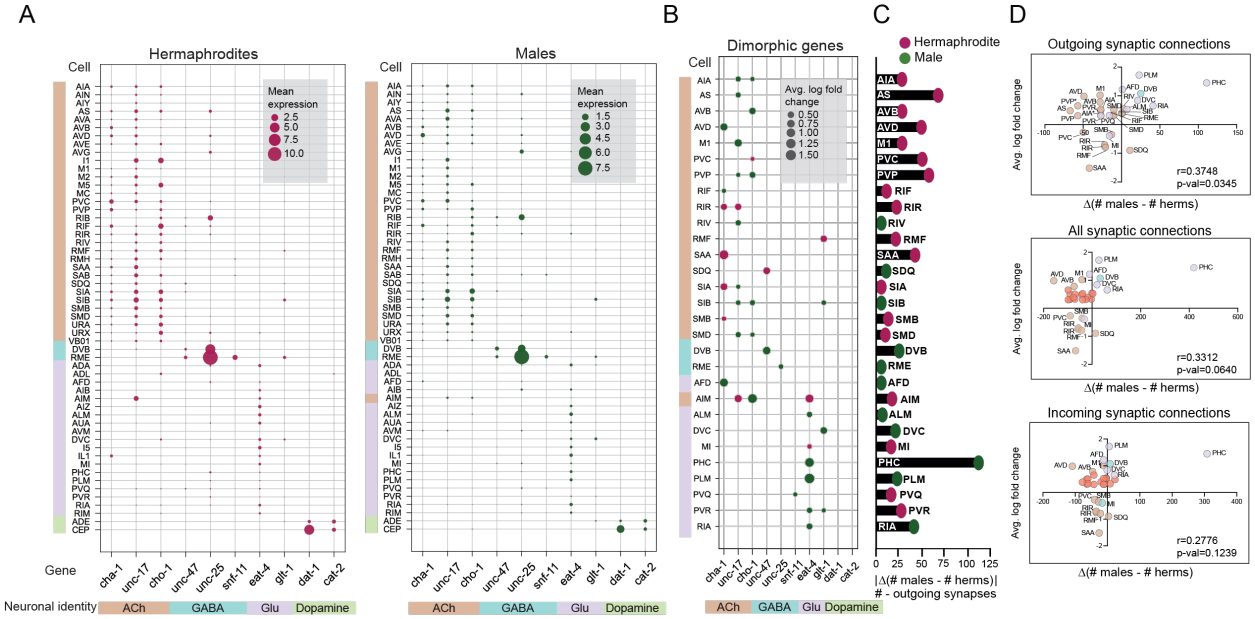

Figure 4. Neurotransmitter identity is preserved across sex-shared neuronal clusters. (A) Left and right bubble plots representing the mean expression values of neuronal identity genes in hermaphrodites and males, respectively. Neuronal clusters and genes are color-coded according to their neurotransmitter identity. (B) Bubble plot representing differentially expressed neurotransmitter identity genes between the sexes. Only genes with significant log fold change are shown. Bubble size in (A) corresponds to gene expression and in (B) to the average log fold change in gene expression. Bubble color indicates enrichment in either sex (green, male; magenta, hermaphrodite). Rows represent neuron types, grouped color coding for neurotransmitter identity. Columns represent individual genes. (C) Bar plot representing the difference in outgoing connectivity between males and hermaphrodites in each cluster. Numbers are represented as an absolute value (*See Methods* for more details). (D) Two-tailed Pearson correlation analysis between the difference in connectivity (outgoing connections, all synaptic connections, and incoming connections) and the average log-fold change of neuronal identity genes (*See Methods* for more details). For (D) we performed a two-sided Pearson correlation test.

Sexually dimorphic gene expression and function of the PLM neuron underlie sex-specific mechanosensory responses

Among the sex-shared neuronal clusters with a high number of DEGs, we observed all the touch receptor neurons (TRNs): ALM, AVM, PVM, and PLM (Figure 2A), required for mechanosensory responses to gentle touch[44]. We turned to explore this dimorphic molecular repertoire, focusing

297 specifically on PLM, a TRN that mediates the posterior gentle touch response[45] and is the most
298 sexually dimorphic among TRNs (Figure 2A, 5A)[44,46]. We validated the differential expression of
299 multiple neuronal-related genes (Figure 5B-C) using transcriptional and translational reporters
300 (Figure 5D-G), or single molecule Fluorescent In Situ Hybridization (smFISH) (Figure 5H). We
301 tested gentle touch responses of hermaphrodites and males. We found that hermaphrodites
302 showed reduced responses to posterior but not to anterior gentle touch (Figure 5I). As a control,
303 we tested harsh touch-tail responses in the same animals[7], which were not dimorphic (Figure 5I).
304 While characterizing the development and growth of PLM, we found sex differences in the length
305 of the posterior processes at the adult stage, with fewer males having posterior processes
306 (Supplementary Figure 7A-D). Analysis of PLM connectivity showed minor differences between
307 the sexes, with males making slightly more gap junctions[35] (Supplementary Figure 7E). Thus, we
308 speculated that the behavioral dimorphism we observed in posterior gentle touch could stem
309 from sex differences in PLM neuronal activity. Indeed, when measuring calcium traces of PLM
310 basal activity, we observed higher activity in males in frequencies up to 2 Hz (Figure 5J-M), further
311 supporting a sexually dimorphic role for PLM. In addition, optogenetic activation of the tail TRNs,
312 which includes PLM, resulted in male behavioral responses that were statistically significantly
313 distinct from hermaphrodites, supporting PLM dimorphism (Supplementary Figure 8). We did not
314 observe significant changes in the expression of major touch-response genes such as *mec-4* and
315 *mec-10*[47,48] (Supplementary Table 2). To test the involvement of specific DEGs in PLM function, we
316 knocked down the neuropeptide *nlp-11* (higher in PLMs of males) or the RNA-binding protein
317 *mec-8* (higher in hermaphrodites) and assayed the RNAi-silenced animals for posterior gentle
318 touch responses in both sexes. While *nlp-11* did not show an effect on gentle touch responses in

319 either of the sexes, *mec-8* was required only in hermaphrodites (Figure 5N). Importantly, over-
320 expressing MEC-8, specifically in PLM, restored the behavioral responses of hermaphrodites
321 (Figure 5O). Altogether, our results establish PLM as a sexually dimorphic neuron with a
322 differential transcriptomic profile and identify a dimorphic gene expression critical for a sex-
323 specific mechanosensory response.

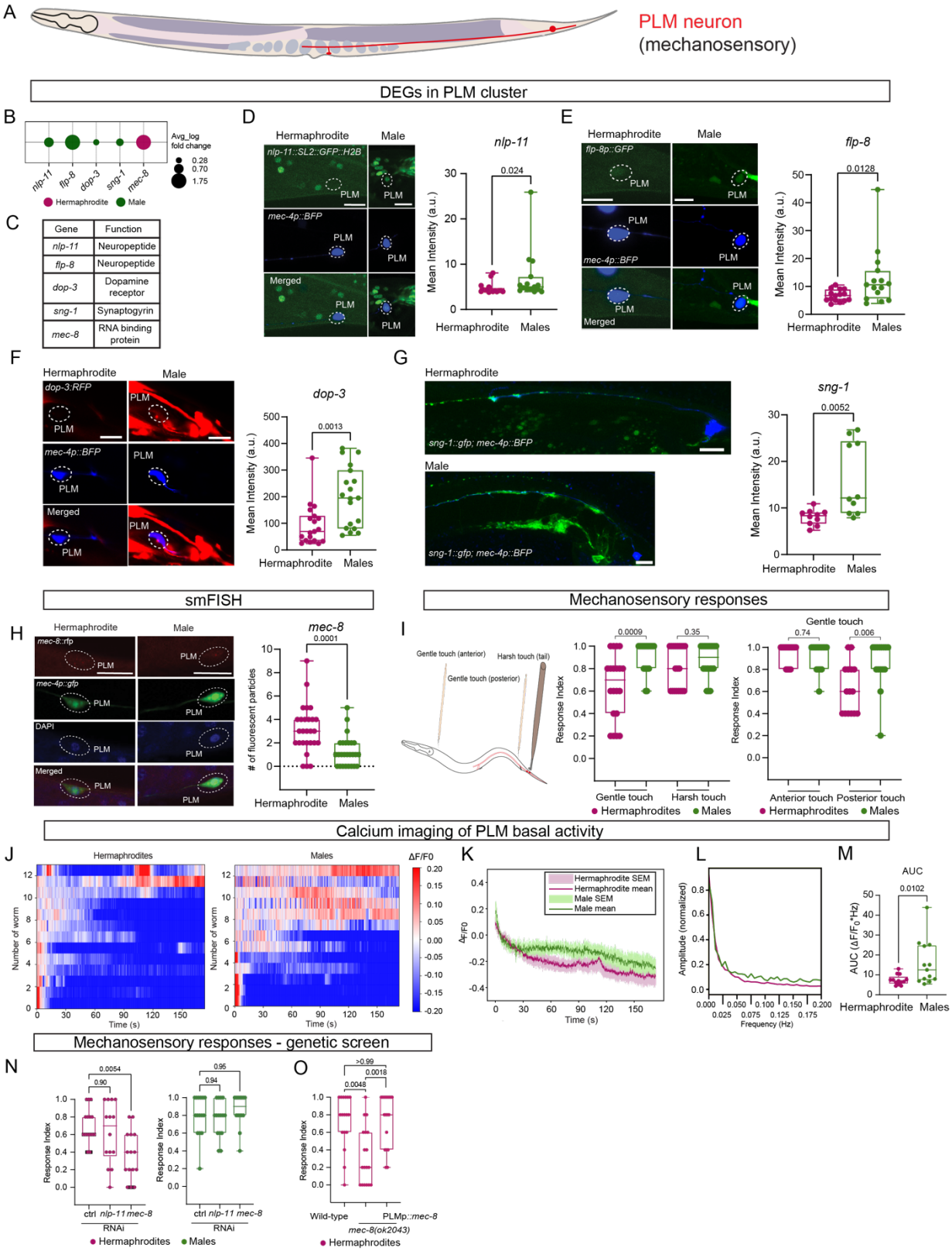
A
PLM neuron
(mechanosensory)
DEGs in PLM cluster
B
Avg_log fold change
0.28
0.70
1.75
nlp-11
flp-8
dop-3
sng-1
mec-8
Hermaphrodite
Male
C
Gene | Function
nlp-11 | Neuropeptide
flp-8 | Neuropeptide
dop-3 | Dopamine receptor
sng-1 | Synaptogyrin
mec-8 | RNA binding protein
D
Hermaphrodite
Male
nlp-11::SL2::GFP::H2B
mec-4p::BFP
Merged
PLM
nlp-11
0.024
Mean Intensity (a.u.)
Hermaphrodite
Males
E
flp-8p::GFP
flp-8
0.0128
F
dop-3:RFP
dop-3
0.0013
G
sng-1::gfp; mec-4p::BFP
sng-1
0.0052
smFISH
H
mec-8::rfp
mec-4p::gfp
DAPI
mec-8
0.0001
# of fluorescent particles
Mechanosensory responses
I
Gentle touch (anterior)
Harsh touch (tail)
Gentle touch (posterior)
Response Index
0.0009
0.35
0.74
0.006
Gentle touch
Harsh touch
Anterior touch
Posterior touch
Hermaphrodites
Males
Calcium imaging of PLM basal activity
J
Hermaphrodites
Males
Number of worm
Time (s)
ΔF/F0
K
Hermaphrodite SEM
Hermaphrodite mean
Male SEM
Male mean
L
Amplitude (normalized)
Frequency (Hz)
M
AUC
0.0102
AUC (ΔF/F0*Hz)
Mechanosensory responses - genetic screen
N
0.0054
0.90
0.95
0.94
Response Index
ctrl
nlp-11
mec-8
RNAi
O
>0.99
0.0018
0.0048
Wild-type
PLMp::mec-8
mec-8(ok2043)

324

Figure 5: Sexually dimorphic properties of the touch receptor neuron PLM. (A) Illustration depicting the positioning of the PLM sensory neuron, as outlined in WormAtlas (https://www.wormatlas.org/) (B) Bubble plot representation of *nlp-11, flp-8, dop-3, sng-1,* and *mec-8* genes expression in PLM clusters of the two sexes. Bubble size represents average log fold change, bubble color (green: males and magenta: hermaphrodites) represents enrichment in either sex. Genes with average log fold change <1 but p-value <0.05 are included. (C) Table lists the established functions of *nlp-11, flp-8, dop-3, sng-1,* and *mec-8* genes. (D) Representative confocal micrographs showing expression of *nlp-11::SL2::GFP::H2B* in PLM neurons (white dotted circle) (left). Quantification of *nlp-11::SL2::GFP::H2B* (right). n = 16 hermaphrodites and 15 males. (E) Representative confocal micrographs showing expression of *flp-8p::GFP* in PLM neurons (white dotted circle) (left). Quantification of *flp-8::GFP* (right). n = 15 animals per group. (F) Representative confocal micrographs showing expression of *dop-3::RFP* in PLM neurons (white dotted circle) (left). Quantification of *dop-3::RFP* (right). n = 19 animals per group. (G) Representative confocal micrographs showing expression of *sng-1::GFP* in PLM neurons (white dotted circle) (left). Quantification of *sng-1::GFP* expression in PLM neurite measured along 100 µm from the soma (right). n = 10 animals per group. (H) Representative confocal micrographs showing expression of *mec-8* CAL Fluor Red 590nm smFISH probe in PLM neurons labeled with *mec-4::gfp* and DAPI (white dotted circle) (left). Quantification of *mec-8* smFISH expression (right). n = 27 hermaphrodites and 26 males. a.u., arbitrary units. Scale bars represent 10 µm. (I) Left: Illustration depicting the gentle touch and harsh touch in the anterior and posterior sides of *C. elegans.* Created with Biorender.com. Middle: posterior gentle touch responses of hermaphrodites and males and harsh tail-touch responses tested on the same animals (n = 20 animals per group). Right: anterior and posterior gentle touch responses of hermaphrodites and males (n=15 animals per group). (J) PLM normalized and color-coded GCaMP6s calcium responses of hermaphrodites and males (n = 13 recordings from 13 animals). Heatmaps represent the calcium levels of individual worms. (K) Mean and SEM traces of PLM calcium responses of hermaphrodites and males. (L) Mean traces showing the normalized amplitudes of PLM, zoomed in at frequencies 0-0.2 Hz. (M) Statistical comparisons of the AUC (area under the curve) measured from PLM amplitudes in the two sexes, for chosen frequencies (0-2 Hz) (*See Methods*). (N) Posterior gentle tail-touch responses of hermaphrodites (left) and males (right) after RNAi knock down of control (n=15 each group), *nlp-11* RNAi (n= 14 for hermaphrodites and n= 15 males), and *mec-8* RNAi (n= 15 for hermaphrodites and n= 14 males). We performed a Kruskal-Wallis test followed by a Dunn's multiple comparison test. (O) Posterior gentle tail-touch responses of hermaphrodites in wild-type (n= 17), *mec-8 (ok2043)* mutant (n=18), and *mec-8* rescue in PLM (n=18). We performed a Kruskal-Wallis test followed by a Dunn's multiple comparison test. In the box-and-whiskers graphs, the center line in the box denotes the median, while the box contains the 25th to 75th percentiles of the dataset, whiskers define the minimum and maximum value with dots showing all points. In (D, E, F, G, H, I, M) we performed a two-sided Mann-Whitney test for each comparison.

The cell adhesion molecule LAD-2 is required for proper neurite extension in male but not hermaphrodite PHC neurons

367 Our study offers molecular candidates to explain the mechanistic basis for previously recognized
368 sexual dimorphism of neurons such as PHC, AFD, AIM and AVG (Figure 2A). For example, we
369 validated two differentially expressed neuropeptides, *flp-7* and *flp-22*, with higher expression in
370 hermaphrodite AVG neurons, suggesting a potential role in modulating AVG's circuit, specifically
371 in hermaphrodites (Supplementary Figure 9)[7]. We next focused on PHC tail sensory neurons,
372 which undergo massive remodeling in males compared to hermaphrodites, with males exhibiting
373 neurite extensions that are twice as long[34]. This elongation is presumably required to
374 accommodate the increased synaptic connectivity with male-specific neurons[34,35] (Figure 6A,
375 Figure 4D). The TF DMD-3 was shown to modify the function, connectivity, and molecular features
376 of the male PHC neurons. We observed increased expression of *dmd-3*, *eat-4/VGLUT* and the
377 neuropeptide *flp-11* in the male PHC cluster[32,34] (Figure 6B). Our ranking analysis identified 209
378 DEGs for PHC (Figure 2A). Supporting the dimorphic connectivity and morphology of PHC, these
379 DEGs were enriched in the GO-terms “synaptic function” and “transmembrane transport” (Figure
380 6C). We validated a subset of neuronal DEGs predicted by our scRNA-seq using transcriptional
381 and translational reporters, including a neuropeptide gene, GABA and dopamine receptors, and
382 the cell adhesion molecule *lad-2* (Figure 6D-I). Since *lad*-2 has been shown to mediate axon
383 guidance[49], we imaged the neurite extension of PHC in both sexes in *lad-2* mutants. We revealed
384 that *lad-2* is required only for the male extension, consistent with its higher expression in males
385 (Figure 6I-K). Taken together, our data set confirms the dimorphic transcriptomic profile for
386 known dimorphic sex-shared neurons and allows the identification and exploration of novel
387 molecular mechanisms within these neurons.

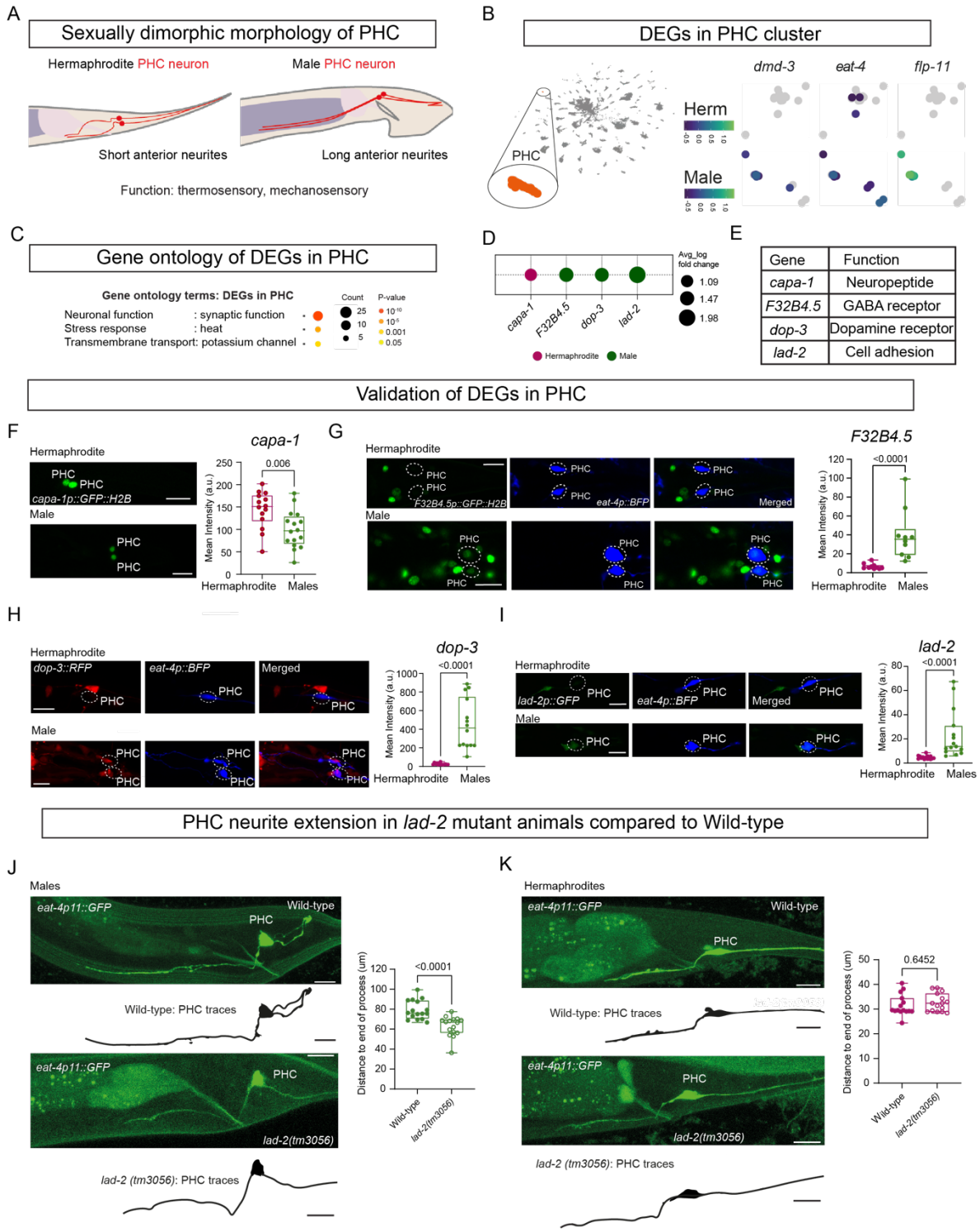

Figure 6: Expression of novel DEGs in PHC. (A) Illustration depicting the location of PHC sensory neurons and their neurite length in both sexes, as outlined in WormAtlas. (B) Validation of previously reported DEGs. Left, PHC representation in the UMAP projection of all cells (inset marked as orange). UMAP projection depicting expression of *dmd-3*, *eat-4*, and *flp-11* gene within PHC cluster. Heatmap represents expression level. (C) GO term enrichments for DEGs in PHC

cluster along with the number of genes in each GO term. (D) Bubble plot representation of *capa-1, F32B4.5, dop-3,* and *lad-2* differential genes expression in PHC cluster. Bubble size represents average log fold change, and bubble color (green: males and magenta: hermaphrodites) represents enrichment in each sex. (E) Table lists the established functions for *capa-1, F32B4.5, dop-3,* and *lad-2* genes. (F) Representative confocal micrographs showing expression of *capa-1p::GFP* in PHC neurons (white dotted circle) (left). Quantification of *capa-1p::GFP* (right). Hermaphrodites, n = 14; males, n= 16. (G) Representative confocal micrographs of *F32B4.5p::GFP* expression in PHC neurons (white dashed circle) (left). Quantification of *F32B4.5p::GFP* (right). n = 10 animals per group. (H) Representative confocal micrographs of *dop-3p::RFP* expression in PHC neurons (white dashed circle) (left). Quantification of *dop-3p::RFP* (right). n = 14 animals per group. (I) Representative confocal micrographs of *lad-2p::GFP* expression in PHC neurons (white dashed circle) (left). Quantification of *lad-2p::GFP* (right). n = 15 animals per group. (J-K) Representative confocal micrographs of *eat-4p11::GFP* expression in PHC neurons in wild-type and *lad-2 (tm3056)* mutant males, n = 16 animals per group (J) and hermaphrodites, n = 10 animals per group (K). Scale bars represent 10 µm. In the box-and-whiskers graph, the center line in the box denotes the median, while the box contains the 25th to 75th percentiles of the dataset, whiskers define the minimum and maximum value with dots showing all points. In (F, G, H, I, J, K) We performed a two-sided Mann-Whitney test for each comparison.

Correlation analysis predicts novel regulators of synaptic connectivity

Can we predict which genes regulate synaptic connectivity based on the relationship between their expression pattern and wiring maps? The relationship between gene expression and synaptic connectivity is a compelling notion in neurobiology. By integrating transcriptomic profiles with connectome data, we can generate predictions on the identity of genes that regulate synaptic wiring. This approach has been previously used, but these studies focused only on hermaphrodites and used binary gene expression data[50,51]. As the connectome of *C. elegans* is available for both sexes, we further utilized our non-binary single-cell gene expression dataset of both sexes and the connectome of *C. elegans* to answer this key question. For this purpose, we calculated the correlation between the number of outgoing connections for each neuron based on[35] and the average gene expression values of all genes in our dataset, across the 62 clusters ranked in Figure 2A, analyzing hermaphrodites and males separately (*See Methods*, Figure 7A-B)[35]. We chose outgoing connectivity because of the availability of pre-synaptic *in-vivo*

426 markers[52,53] for further validation of candidates. To identify genes that might regulate the
427 outward connectivity of neurons, we performed statistical analysis accounting for multiple
428 comparisons, which resulted in an adjusted p-value for each correlation value (*See Methods*). We
429 then searched for significantly correlated genes that overlap between hermaphrodite and male
430 correlation profiles (Figure 7C). We discovered 54 genes with significant correlation in both sexes,
431 with more than half still uncharacterized. Among the neuronal genes exhibiting a significant
432 positive correlation, are key presynaptic genes such as the active zone scaffold *syd-2* involved in
433 presynaptic assembly [54,55], but also postsynaptic genes such as *acc-2,* encoding acetylcholine-
434 gated chloride channel[56], and *gar-3* encoding G-protein-linked acetylcholine receptor[57] (Figure
435 7C). This finding highlights numerous uncharacterized genes with potential synaptic function and
436 suggests that some synaptic regulatory pathways are shared between the two sexes. To gain a
437 better perspective into dimorphic synaptic regulation, we looked specifically for neuronal genes
438 that are either significantly correlated with outgoing connectivity in hermaphrodites, in males or
439 in both sexes (Figure 7D). While exploring the expression of these genes in our data set, we
440 uncovered the sexually dimorphic expression patterns of some of them (Figure 7E). Importantly,
441 these genes included *ttx-7,* which encodes a myo-inositol monophosphatase (IMPase), already
442 shown to mediate proper synaptic localization in the interneuron RIA[58] and *zig-1* predicted to
443 encode a cell adhesion molecule whose function is unexplored[59,60]. We found that *ttx-7* is
444 significantly correlated in both sexes (Figure 7C). Based on *ttx-7* expression profile, we
445 hypothesized that it might regulate synaptic connectivity of RIA neurons in both sexes (since both
446 express it equally high), but its absence would have a greater effect on the synaptic connectivity
447 of hermaphrodites CEP neurons (since it is highly expressed in hermaphrodites) (Figure 7E, red

448 squares, and 7F). We indeed found that in *ttx-7* mutant animals, RIA pre-synapses were mostly
449 mislocalized in both sexes (Figure 7G), while the number of pre-synapses in CEP neurons was
450 reduced only in hermaphrodites (Figure 7I). *zig-1* mutant animals showed lower pre-synaptic
451 signal only in males, in concordance with the gene being significantly correlated only in males
452 (Figure 7D, Figure 7H). We conclude that combining our dataset together with connectivity maps
453 uncovers novel genes regulating synaptic wiring, both in non-dimorphic and dimorphic contexts.

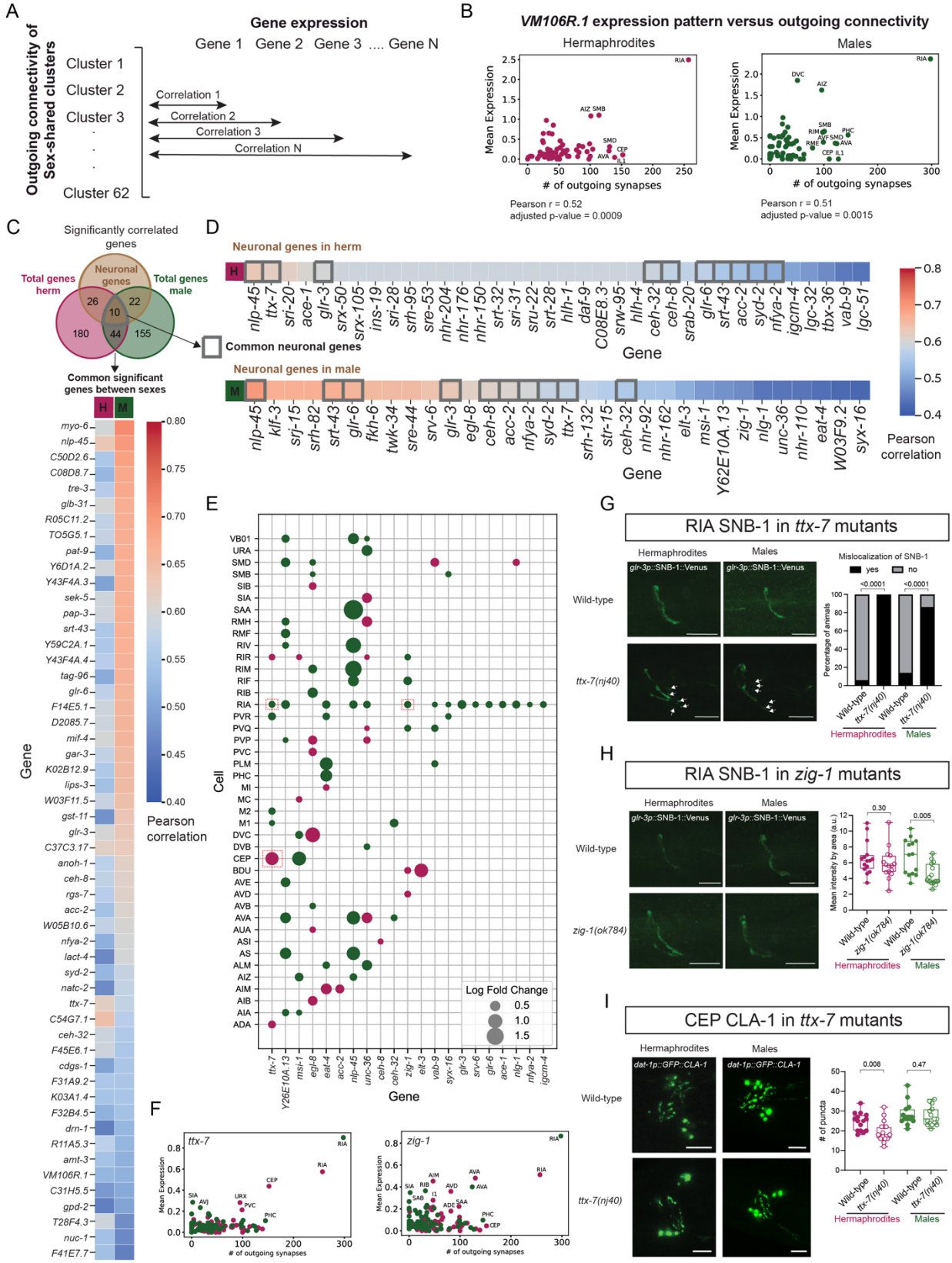
A
Gene expression
Gene 1 Gene 2 Gene 3 .... Gene N
Outgoing connectivity of Sex-shared clusters
Cluster 1
Cluster 2
Cluster 3
Cluster 62
Correlation 1
Correlation 2
Correlation 3
Correlation N
B
VM106R.1 expression pattern versus outgoing connectivity
Hermaphrodites
Males
Mean Expression
# of outgoing synapses
Pearson r = 0.52
adjusted p-value = 0.0009
Pearson r = 0.51
adjusted p-value = 0.0015
C
Significantly correlated genes
Total genes herm
Neuronal genes
Total genes male
Common neuronal genes
Common significant genes between sexes
Gene
Pearson correlation
D
Neuronal genes in herm
Neuronal genes in male
Common neuronal genes
Gene
Pearson correlation
E
Cell
Gene
Log Fold Change
F
ttx-7
zig-1
Mean Expression
# of outgoing synapses
G
RIA SNB-1 in ttx-7 mutants
Hermaphrodites
Males
Wild-type
ttx-7(nj40)
Mislocalization of SNB-1
yes
no
Percentage of animals
H
RIA SNB-1 in zig-1 mutants
zig-1(ok784)
Mean intensity by area (a.u.)
I
CEP CLA-1 in ttx-7 mutants
# of puncta

454

455 **Figure 7. Correlation analysis identifies novel genes that regulate synaptic connectivity.** (A)
456 Schematic of the correlation analysis. Rows represent the number of outgoing synaptic
457 connections calculated according to[35] (*See Methods*) across neuronal clusters, and columns
458 represent genes and their mean expression values across neuronal clusters. Pearson correlation
459 is calculated between connectivity numbers and mean gene expression for each gene. This
460 analysis was done separately for the hermaphrodite and male data sets. (B) an example of the
461 correlation output. Scatter plots representing the mean expression of the significantly correlated
462 gene *VM106R.1* across the number of outgoing connections in males (right) and hermaphrodites
463 (left). Each dot in the scatter plot represents a neuronal cluster. (C) Venn diagram showing
464 significantly correlated genes in hermaphrodites (magenta) and in males (green) and the number
465 of neuronal genes within these two groups (brown) (top). Heatmap of the Pearson correlation
466 coefficients of the significantly correlated and overlapping genes between hermaphrodites and
467 males (bottom). (D) Heatmaps of the Pearson correlation coefficient of significantly correlated
468 neuronal genes in hermaphrodites (top) and in males (bottom). Common genes in both data sets
469 are marked with a gray square. (E) Bubble plot representation of differential gene expression
470 across neuronal clusters of the neuronal genes from (D). Bubble size represents average log fold
471 change, bubble color (green: males and magenta: hermaphrodites) represents enrichment in
472 each sex. Only significant DEGs are shown. Red square refers to genes and cells analyzed in (G-I).
473 (F) Scatter plots representing the mean expression of *zig-1* (right) and *ttx-7* (left) across the
474 number of outgoing connections in hermaphrodites (magenta dots) and males (green dots). Each
475 dot in the scatter plot represents a neuron. (G) Representative confocal micrographs of *glr-*
476 *3p::SNB-1::venus* expression in RIA neurons in wild-type and *ttx-7(nj40)* mutant hermaphrodites
477 and males (left). Percentage of animals showing mislocalization signal of SNB-1 in RIA (right).
478 Wild-type hermaphrodites n = 15, Wild-type males n = 14, *ttx-7(nj40)* n = 15 per group. (H)
479 Representative confocal micrographs of *glr-3p::SNB-1::venus* expression in RIA neurons in wild-
480 type and *zig-1(ok784)* mutant hermaphrodites and males (left). Quantification of venus signal in
481 RIA (right). a.u., arbitrary units. Wild-type hermaphrodites n = 15, Wild-type males n = 14, *zig-*
482 *1(ok784)* n = 15 per group. (I) Representative confocal micrographs of *dat-1::novogfp::CLA-1*
483 expression in CEP neurons in wild-type and *ttx-7(nj40)* mutant hermaphrodites and males (left).
484 Quantification of CLA-1 puncta in CEP (right). n = 15 per group. In the box-and-whiskers graphs,
485 the center line in the box denotes the median, while the box contains the 25th to 75th percentiles
486 of the dataset, whiskers define the minimum and maximum value with dots showing all points.
487 For (C) we performed Pearson correlation analysis with Benjamini Hochberg correction for
488 multiple comparisons (*See Methods*). For (G) we performed a two-sided Fisher's exact for each
489 comparison. For (H-I) we performed a two-sided Mann-Whitney test for each comparison.
490

491 **DISCUSSION**

492 In this work, we established a comprehensive transcriptome map of the sex-shared nervous
493 system in both sexes and uncovered novel sexually dimorphic neurons, including the posterior
494 light touch neurons PLM. In addition to sex-shared neurons, *C. elegans* males have an additional

495 93 male-specific neurons. Even though these can be subdivided into neuronal subtypes[42,61], for
496 most male specific-neurons molecular markers that define individual identities haven't been
497 described. Thus, male-specific clusters have been left out of this analysis, until further tools
498 become available[62]. Our ranking analysis reveals that the most prominent dimorphic gene family
499 is neuropeptides, with a male-biased expression, in accordance with our previously published
500 developmental comparison between the sexes[31]. Neuropeptides are short protein ligands that
501 modulate synaptic activity mostly through the binding to G protein-coupled receptors (GPCRs),
502 playing a critical role in regulating functions of the nervous system functions[63]. A
503 neuropeptidergic connectome has recently been constructed, revealing a dense network with
504 unique sex-shared neurons that serve as "peptidergic hubs"[64]. This suggests that a significant
505 rewiring of the neuropeptidergic connectome occurs in addition to the rewiring of the physical
506 connectome between sexes. Future studies exploring the entire neuropeptidergic connectome in
507 sexually dimorphic context would shed more light on how neuropeptide signaling has diverged to
508 drive nervous system function and behavior. [31,65].
509 Our functional analysis of sex-shared neurons uncovers a novel sexual dimorphism in
510 mechanosensory posterior gentle touch responses, with males displaying higher sensitivity
511 compared to hermaphrodites. This difference is likely mediated by the highly dimorphic touch
512 receptor neuron PLM, which exhibits significant differences in basal neuronal activity between
513 the sexes. While PLM activity decreases when courtship begins[66], the heightened
514 mechanosensory responses in males may be essential for mating, as was already shown for
515 turning behavior[68]. Hermaphrodites, on the other hand, do not display such behavior and show
516 lower sensitivity. In contrast, both sexes exhibit similar responses to harsh tail touch[7], suggesting

517 that hermaphrodites maintain robust responses to dangerous stimuli for survival. Our focus on
518 mechanosensation in this and previous work[7] provides insights into how different touch
519 modalities (gentle and harsh) can result in distinct outcomes, potentially reflecting different
520 evolutionary pressures.

521 We identified the RNA binding protein MEC-8 as a hermaphrodite-enriched gene in PLM and
522 shown it to be critical for their PLM mechanosensory responses, suggesting that different
523 molecular mechanisms mediate mechanosensation in the two sexes.

524 Our single-cell data set identified the cell adhesion molecule LAD-2 as a male-specific regulator
525 of PHC neurite extension[34], though which specific isoform is responsible remains unclear[69]. Future
526 screens are required to uncover genes governing PHC neurite structure in hermaphrodites.

527 We observed that neurotransmitter identity is largely preserved across sexes, with the notable
528 exception of AIM neurons. Slight changes in expression levels for neurotransmitter genes
529 between the sexes correlate with changes in outgoing connectivity, although this correlation was
530 relatively low (r=0.37), suggesting other factors might underlie the differences in outgoing
531 connectivity, such as synaptic-related genes, transcription factors, or a combination between
532 different genes. This led us to explore the correlation between gene expression across our data
533 set and connectivity. Based on this, we were able to predict a large number of candidate genes in
534 both sexes that might regulate outgoing connectivity, validating two of them. While this
535 correlation analysis was sufficient to identify gene-to-connectivity matches for specific neurons,
536 it could not be extended to the entire worm's nervous system, as our analysis did not capture all
537 sex-shared neurons (62 clusters that have passed all the filters in ranking analysis) and some of
538 the sex-shared neurons are under-represented in our data set. Further studies profiling the rest

539 of the sex-shared neurons will possibly allow for a more accurate prediction of the way gene
540 expression regulates connectivity. Even with a full transcriptomic representation of the nervous
541 system, predictions can be complicated due to interactions existing between genes and to
542 differences between connectivity and single-cell RNA sequencing data pooling (small sample size
543 in EM sections versus pooling large number of worms for single-cell).
544 Overall, our integrative approach, combining molecular, cellular, behavioral, and computational
545 analyses, provides significant insights into sexual dimorphisms within the sex-shared nervous
546 system. This work lays the ground for future studies aimed at uncovering novel molecular
547 programs that regulate these neuronal dimorphisms, with implications for understanding similar
548 processes in higher organisms and the development of gender-specific therapeutic strategies.
549

550 **METHODS**

551 ***C. elegans* strains and maintenance**

552 All *C. elegans* strains used in this study were cultivated according to standard methods[70]. Wild-
553 type strains were Bristol, N2. *him-5(e1490)* or *him-8(e1489)* were treated as controls for strains
554 with these alleles in their background. Worms were grown on nematode growth media (NGM)
555 plates seeded with *E. coli* OP50/NA22 bacteria as a food source. Worms were raised at 20°C,
556 unless noted otherwise. The sex and age of the animals used in each experiment are noted in the
557 associated figures and legends. All transgenic strains used in this study are listed in the key
558 resources table.

559 **Isolation of *C. elegans* pure male population**

560 To generate pure male populations, we followed our previously described protocol[31]. Briefly, *C.*
561 *elegans* strain with the genotype *rab-3p(prom1)::2xNLS::TagRFP] IV; dpy-28(y1) III; him-8(e1489)*
562 *IV* was employed. This strain harbors a temperature-sensitive mutation (*y1*) in the dosage
563 compensation gene, *dpy-28* along with *him-8(e1489)* mutation and a pan-neuronal RFP. Worms
564 were cultured at 15°C on 15 cm NGM plates seeded with NA22 bacteria. Embryos were isolated
565 by hypochlorite treatment and were age-synchronised 14-16 hours on a foodless NGM plate at
566 25°C. L1 larvae were collected and were placed on a food NGM plates approximately 1.5 cm from
567 the food on NGM plates and were allowed to crawl towards food for 1-2 hours at RT. Using a
568 scalpel, the area where L1/embryos were initially placed was removed. L1 worms were collected
569 and washed with M9 buffer and were incubated at 20°C until adulthood. This resulted in male
570 population of ≥98% purity. For each experiment the percentage of males in the population was
571 recorded.

572 **Worm single cell dissociation**

573 Worms of the desired genotype were grown at 15°C on 15 cm NGM plates seeded with NA22
574 bacteria until the plates were populated. Gravid adult worms were collected in M9 buffer and
575 embryos were isolated by hypochlorite treatment. The obtained embryos were hatched for 14-
576 16 hours on a foodless NGM plate at a restrictive temperature of 25°C. The number of L1 larvae
577 were counted and were plated (40,000-50,000 animals per plate) on a fresh NA22 seeded
578 bacterial plates and were grown to young adult stage at 20°C. Young adult worms were washed
579 10 times at 1300 rpm for 2 minutes with M9 buffer to get rid of any adhering bacteria. The worms
580 were then washed with ddH_2O. The worm pellets were then subjected to single cell dissociation
581 using protocols described earlier with slight modifications[20,71–74]. For every 0.5 ml of worm pellet

582 1 ml of freshly thawed sterile SDS-DTT solution (200 mM DTT, 0.25% SDS, 20 mM HEPES, 3%
583 sucrose, pH 8.0, thawed freshly) was added and incubated at room temperature for 4 min with
584 gentle mixing every 1 minute. Immediately after SDS-DTT treatment, worms were pelleted at
585 3,000 rpm for 1 min and washed 5 times with 10 ml egg buffer (118 mM NaCl, 48 mM KCl, 2 mM
586 $CaCl_2$, 2 mM $MgCl_2$, 25 mM HEPES, pH 7.3). 0.5 ml aliquots of worm pellet were distributed to 1.6
587 mL microcentrifuge tubes. 1 mL freshly prepared 15 mg/mL Pronase-E was added to each tube
588 and flicked to mix and then rotated at 20°C for 5 minutes. Using a glass pasteur pipette, worm
589 suspensions were combined from multiple tubes and were transferred to a 7 mL dounce
590 homogenizer (pestle clearance 0.02−0.056 mm, Kimble Chase). Pronase E was added to a final
591 ratio of 4:1 relative to the worm pellet. If the worm pellet was smaller than 0.5 mL a 2mL glass
592 homogenizer was used. The animals were disintegrated to single cells using type "B" plunger for
593 4-5 minutes at room temperature and then continued on ice gently. We note that homogenizing
594 on ice increased cell survival. The status of dissociation was monitored under a dissecting
595 microscope at 5-minute intervals. Dissociation was stopped when most of the animals were
596 dissociated but a few whole or fragmented animals were still present. Using a glass pasteur
597 pipette the cell suspension was aliquoted into 1.6 mL microcentrifuge tubes that were centrifuged
598 at 5,000 x g for 5 minutes at 4 °C. Supernatant was removed and the cell pellet was washed 3
599 times with 1 mL ice-cold egg buffer per wash at 5,000 x g for 5 minutes at 4 °C. The cells pellet
600 was resuspended in 1 ml ice-cold egg buffer and was passed through 5 µm syringe filter gently.
601 Cell suspension was taken on ice to FACS sorting immediately.

602 **FACS based sorting**

603 Single cell suspension from the desired strain were subjected to Fluorescence Activated Cell
604 Sorting (FACS) on a BD FACSAria™ III Cell Sorter using a 70-micron nozzle. eFlour 450 dye (final
605 concentration of 1 µl/mL) was used to discriminate live and dead cells. The cells were gated for
606 side scatter (SSC)-Area vs forward scatter (FSC)-Area, then single cells were selected from doublet
607 using FSC-Height vs FSC-Area. Finally, RFP+ cells were gated and sorted under the "4-way Purity"
608 mask from this subpopulation. Wild-type *him-5(e1490)* without any RPF+ cells was used as
609 control for gating. Sorted cells were collected in 1.6 mL microcentrifuge tube containing 500 µl L-
610 15-20 (L-15 medium containing 20% fetal bovine serum). The suspension was centrifuged at 5,000
611 x g for 10 minutes at 4 °C, resuspended in 50-80 µl of L-15-20 and counted using a
612 hemocytometer.

613 **RT-PCR**

614 For carrying RT-PCR experiments a previously described protocol was used[31]. YA hermaphrodite
615 worms were dissociated into single cells and the RFP+ and RFP- cells were FACS sorted in 500 µL
616 Trizol, flash frozen in liquid nitrogen and stored at -80°C until further processing. Total RNA was
617 extracted using the TRIzol LS (Invitrogen) protocol until the isopropanol precipitation step then
618 was re-suspended in the extraction buffer from RNA isolation kit (PicoPure, Arcturus). The
619 manufacturer's recommendations were followed for further isolation. Using the SuperScript™ IV
620 first-strand synthesis system (Invitrogen, Catalog # 18091050) and random hexamers, the
621 extracted total RNA was then converted to cDNA. Fast SYBR™ Green Master Mix (Applied
622 Biosystems, Catalog # 4385612) was used to carry out qPCR as per manufacturer protocol. The
623 experiments were carried out in 3 biological replicates. *act-1, pmp-3* and *tba-1* genes served as

624 internal controls. Ct values were obtained, and relative quantification of the expression of the
625 target genes was performed utilizing 2−ΔΔCt method.

626 **Cell imaging (imaging flow cytometer)**

627 Cell imaging experiments were carried out using an ImageStreamX Flow Imager system to
628 evaluate the morphology and viability of cells after single cell dissociation. Single cells were
629 dissociated from a *C. elegans* strain expressing pan-neuronal TagRFP as described above and were
630 resuspended in PBS with eFlour 450 dye (Live/Dead) and DRAQ5 dye (DNA binding) to a final
631 concentration of 1 µl/mL. The positive samples containing all fluorochromes were used to set up
632 each channel and the laser intensities. Gating was conducted based on Area vs RFP intensity,
633 followed by the selection of RFP+ cells and by discriminating fluorophore using Area vs intensity.
634 Cells derived from Wild-type N2 without RFP+ expression served as a control for gating. Images
635 were acquired for 20,000 cells.

636 **Single-cell RNA sequencing**

637 Depending upon the cell concentration, the single-cell suspensions were diluted to reach the
638 optimal range as recommended by 10x genomics manufacturer's protocol (approx. 800-1000
639 cells/µl). Each lane in the 10x genomics chip was targeted for 8,000 or 10,000 cells. Libraries were
640 prepared with 10x Genomics v3 Chemistry according to the manufacturer's protocol. The libraries
641 were sequenced using the Illumina NovaSeq 6000 with 150 bp paired end reads, except for one
642 hermaphrodite sample which was sequenced using the Illumina Nextseq 500 with a 75 cycle high
643 output kit and paired end sequencing. Detailed experimental information is found in
644 Supplementary Table 3. Real-Time Analysis software (RTA, version 4.0.0; Illumina) was used for

645 base calling and analysis was completed using 10X Genomics Cell Ranger software (4.0.0).
646 Detailed experimental information is found in Supplementary Table 3.

647 **Single-cell RNA-Seq Mapping**

648 Sequenced reads from each experiment were mapped to the *C. elegans* reference transcriptome,
649 version WBcel235 release WS276, using the Cell Ranger pipeline version 4.0.0. We extended the
650 3' UTR of each gene by 500 base pairs for additional mapping of reads to the 3' extremity of the
651 gene body since the 3' end is poorly annotated in *C. elegans*[26].

652 **Background correction and filtering procedure**

653 For each experimental batch (6 hermaphrodite and 6 male samples), the empty droplets were
654 identified and background correction was performed using SoupX[75] as previously described[20].
655 Subsequently, a cell filtering step on each batch was performed followed by clustering cells in
656 UMAP space using Seurat using 50 PCs (Supplementary Figure 10A). Clusters were defined by
657 computing Shared Nearest Neighbor using only the first two UMAP dimensions and the original
658 Louvain algorithm with a resolution of 1, using FindNeighbors and FindCluster functions where
659 all other parameters were set to default. Clusters with more than 0.5% neuronal markers and less
660 than 1.5% non-neuronal markers were selected for further analysis (Supplementary Figure 10B)
661 using a list of 563 neuronal and 114 non-neuronal marker genes based on Supplementary Table
662 1. To ensure no loss of neurons through this procedure, a second round of selection was
663 performed on cells that did not pass the first filtering step. For the second round, subclustering
664 was performed on the remaining clusters using same parameters as before and the same filtering
665 of clusters using neuronal and non-neuronal markers was applied. Finally, cells containing more

666 than 20% of UMIs originating from mitochondrial genes were removed (Supplementary Figure
667 10D-E).

668 **Dimensionality reduction, batch correction and cluster Identification**

669 Monocle 3 was used to combine the male and female batches with the CenGEN[20] L4
670 hermaphrodite neuronal data. Counts were imported to Monocle 3 and batches were aligned
671 using Batchelor using 135 PCs and an alignment k of 5, followed by UMAP dimensional reduction
672 using a minimal distance of 0.3 and 75 neighbors, and clustering using Leiden algorithm with a
673 resolution of 3e-3, resulting in 72 partitions. This UMAP projection was kept to display the final
674 clustering and annotation analysis. Two iterative rounds of subclustering were performed after
675 the first one. For the second iteration 2 subclustering steps were performed on partition 1 and on
676 the merge of partitions 2 to 72. The same parameters were used for both subclusterings: 135 PCs
677 and an alignment k of 20, followed by UMAP dimensional reduction using a minimal distance of
678 0.1 and 15 neighbors, and clustering using Leiden algorithm with a resolution of 3e-4 resulting in
679 36 and 82 new partitions, coming from former partitions 1 and 2-72, respectively. This totaled
680 118 partitions that were inspected to assign identities or to continue with a third round of
681 sublcustering. The third iteration of subclustering was only applied to partitions where identity
682 was not well defined after two iterations. We used partition definition in Monocle 3 to define
683 clusters that were well segregated and with identities well defined based on the content of
684 CenGEN annotated cells. If these partitions contained mixed CenGEN identities in some cases we
685 opted for the cluster definition if the segregation of cells matched well with a single neuronal
686 identity. In other cases, a third round of dimensionality reduction and clustering was performed.
687 In total, 27 partitions from the second iteration underwent a third round of subclustering,

688 producing a total number of 156 cell partitions/clusters. Finally, the CenGEN annotated cells
689 included in the clusters were used to annotate the clusters.

690 **Pairwise comparison of clusters**

691 To compare the similarity of gene expression between our hermaphrodite dataset and the
692 hermaphrodite L4 dataset generated by CenGEN, we used the 5000 most variable genes in our
693 dataset to calculate the Spearman correlation of the cell cluster using their average gene
694 expression. The results were plotted in a clustered heat map where the complete-linkage
695 clustering method was calculated for rows and columns using euclidean distances.

696 **Differentially expressed gene analysis**

697 Several metrics were extracted for all genes and all cells, including expression fraction and
698 average expression (Supplementary Tables 6-7). Differentially expressed genes between
699 hermaphrodite and male neurons for each cluster was performed using Seurat's "FindMarkers"
700 function with default parameters on log-normalized dataset. The thresholds were set to include
701 testing only genes detected in a minimum fraction of cells in either of the two populations, with
702 a default value of 0.01, and limiting testing to genes that show, on average, at least a 0.1-fold
703 difference (log-scale) between the two groups of cells, which is also the default value of
704 FindMarkers function. Finally, this step provided natural log fold changes, percentage of cells
705 where gene is detected for each sex and p value statistics provided by Wilcoxon Rank Sum test
706 (Supplementary Table 2).

707 **Thresholding of gene expression**

708 In order to define gene expression across neuron types we used the same thresholding strategy
709 as Taylor, S. R. *et al.* [20]. First, we defined how many cells should a cluster have in order to poses

710 similar predictive capabilities. For this, we generated Receiver-Operator Characteristic (ROC)
711 curve of True Positive Rate (TPR) vs False Positive Rate (FPR) by comparing the single-cell data to
712 the ground truth. As the ground truth dataset, we used the expression patterns of 160 neuronal
713 genes determined with high confidence in adult hermaphrodite, as previously described[20,38,76–79].
714 For this purpose, we assumed expression when the fraction of cells expressing was bigger than 0
715 and we found that using clusters with 9 cells or more in both sexes (65 cell types) give similar
716 predictive power when compared to CenGEN dataset (Figure 1D). With this in mind, we used
717 these 65 cell types to define the thresholding of the whole dataset following the same steps as
718 described in Taylor, S. R. *et al.*[20]. We used the proportion of cells in which a gene was detected to
719 define thresholds where genes identified in at least 1% of the cells within each neuron cluster
720 were regarded as expressed across all types of neurons, whereas transcripts detected in no more
721 than 2% of the cells within each neuron cluster were regarded as non-neuronal. In the case of
722 other genes, we implemented the percentile thresholding on a gene-by-gene basis, determining
723 thresholds as a fraction of the highest cell proportion observed for each gene. Using the R package
724 boot[80–82], we produced 5,000 stratified bootstraps of the ground truth genes for each threshold
725 percentile. Subsequently, we determined the TPR, FPR, and False Discovery Rate (FDR) for the 57
726 clusters and for each distinct neuron type (Figure 1D-E). We used the same 4 thresholds of
727 increasing stringency and in these 57 clusters, we observed similar performance as reported
728 before for the whole L4 dataset (Figure 1E). Finally, this thresholding was used for other clusters
729 even if they contained 10 cells or less.

730 **Ranking analysis**

731 To rank the sex-shared neuronal clusters according to the number of differentially expressed
732 genes (DEGs) between the sexes, we counted the number of DEGs in each cluster using Python
733 3.12. Clusters with mixed or unknown identities were removed from this analysis because of
734 inability to calculate connectivity numbers for these clusters for the analysis below. Clusters were
735 included only if there were more than 9 cells in a cluster for both sexes. This yielded a list of 62
736 sex-shared clusters we continued analyzing (Supplementary Table 4). A gene was considered as
737 differentially expressed if the following criteria were met: average log fold change > 1, p-value <
738 0.05, threshold ≥ 2 in at least one sex (in order not to exclude genes with no expression in one
739 sex and high expression in the other). Then, the number of DEGs received after filtering (2216)
740 was used to generate gene ontology analysis, calculate the fraction of DEGs per gene family and
741 the number of sex-biased DEGs according to gene family (Figure 2B-D) and bubble plots
742 representing differential expression of specific gene families (Figure 3A, Supplementary Figure 5,
743 Supplementary Figure 6) were generated using GraphPad prism 10.

744 **Sex-bias of differentially expressed genes across gene families**

745 Using Python 3.12, we calculated the number of DEGs in males and in herms separately according
746 to gene families (see gene families in Figure 2D) for all the DEGs between the sexes that passed
747 the filter (Figure 2A). If a gene appeared in multiple clusters as a DEG, it was counted according
748 to the number of clusters it appeared. For example, *flp-7* is DE in the clusters AVG, RMF and URX,
749 so it was counted three times. For statistical analysis, we performed Fisher's exact test for each
750 gene family (subtracting the number of each count in each sex from the total count of genes in
751 all families included in the analysis) and then corrected with Bonferroni by multiplying each p-
752 value by the number of comparisons.

753 **Neurotransmitter identity analysis**

754 To analyze the expression of neurotransmitter genes in our data set, we used Python 3.12,
755 generating expression bubble plots for the two sexes separately (Figure 4A-B, using
756 Supplementary Tables 6-7, mean expression values of hermaphrodites and males respectively
757 across sex-shared clusters) and for dimorphic expression of neuronal identity genes (Figure 4C).
758 The clusters used for this analysis are listed in Supplementary Table 4. Then, to calculate the
759 connectivity of the sex-shared neuronal clusters we used Supplementary information 3 from
760 Cook, SJ. *et al.*[35]. This calculation included only connectivity observed by the electron microscopy
761 (EM) reconstructions[35]. For each cluster, we calculated using Python 3.12 for each sex the number
762 of outgoing connections (when the neuron is pre-synaptic), the number of incoming connections
763 (when the neuron is post-synaptic) and the sum of these two calculations (all synaptic
764 connections, chemical connections) (Supplementary Table 5). For our analysis we combined left
765 and right connectivity numbers for each neuron. Then, we calculated the difference between the
766 number of male connections and the number of hermaphrodite connections in each cluster, for
767 each synaptic category. These numbers are represented in Figure 4C as an absolute number. To
768 correlate the difference in connectivity with average log fold change of neurotransmitter identity
769 genes (Supplementary Table 2), we used two-tailed Pearson correlation analysis in GraphPad
770 Prism 10. We did this analysis for every synapse category (outgoing, incoming and all). Clusters
771 with two neurotransmitter identity genes showing dimorphic expression were included twice in
772 the correlation analysis. SIA cluster was discarded because the two neurotransmitter identity
773 genes were showing different sex biases (*cha-1* higher in hermaphrodites and *unc-17* higher in

774 males). AIM was also discarded because its neurotransmitter identity is known to be dimorphic,
775 being glutamatergic in hermaphrodites and cholinergic in males in the adult stage[33].

776 **Microscopy**

777 Confocal images were acquired using Zeiss LSM 880 confocal microscope using 20x, 40x or 63x oil
778 immersion objectives. Worms were anaesthetized in sodium azide (NaN3, final concentration 200
779 mM, prepared in M9 buffer) and mounted on a 5 % agarose pad (freshly prepared) on a glass
780 slide. The images were processed using ImageJ/Fiji software version 2.3.0/1.53q[83] or Zen
781 software. All images of the same group were imaged using identical microscope settings. Figures
782 were prepared using Adobe Illustrator v24.2.1. For imaging NeuroPAL worms, channels were
783 pseudo-colored in accordance with ref[38,39]. For single neuron expression quantification, ROIs were
784 chosen manually at the z-plane with the strongest signal using the respective fluorescent marker.
785 For *sng-1::GFP* analysis we measured the fluorescence intensity of the signal in PLM neurite
786 (observed by *mec-4p::*BFP) measured along 100 µm from the soma. For PLM development
787 analysis we measured the length of the anterior and posterior neurites using *mec-4p::BFP*
788 labeling. For Figure 6J-K we measured the length of PHC neurite from the anus which is visible
789 through *eat-4p11::GFP*. For Supplementary Figure 9 we identified AVG based on its anatomic
790 position and shape. For Figure 7G we calculated the percentage of animals with mislocalized
791 signal of *SNB-1::Venus* and for Figure 7H we measured *SNB::Venus* signal by manually selecting
792 ROI and normalizing the mean intensity value received to its area for each animal. For Figure 7I
793 we counted the number of CLA-1 puncta that surround CEP neurons.

794 **Neuron identification using NeuroPAL**

795 For neuronal identification the relevant CRISPR GFP reporters were crossed with NeuroPAL
796 landmark strain OH15262 harboring *otIs669* transgene. For imaging NeuroPAL worms, the
797 protocol followed are in accordance with ref[38,39]. For CRISPR GFP neuronal identity, colocalization
798 with the NeuroPAL landmark strain OH15262 harboring *otIs669* transgene was used to determine
799 the identity of all neuronal expression. Using ImageJ version 1.52p, the z-plane with the strongest
800 signal was used to measure the fluorescence intensity of individual neurons that were identified
801 by reporter/stain expression.

802 **Gene ontology analysis**

803 The WormCat gene set enrichment analysis tool was used for functional annotation of gene
804 ontology terms that are over-represented in differentially expressed genes combined or for each
805 sex[84].

806 **Molecular cloning**

807 To generate *mec-4p::BFP* and *eat-4p11::BFP* for PLM and PHC visualization we used PCR fusion[85].
808 *mec-4p* was amplified from *mec-4p::GCaMP3::tagRFP* kindly provided by Alon Zaslaver, while *eat-*
809 *4p11* was amplified from an eat-4p11 containing plasmid. *BFP* fragment was amplified from a
810 plasmid containing *flp-6::tagBFP* kindly provided by Hannes Bulow. To generate PLM specific
811 rescue of MEC-8, *F10A3.11* promoter (460 bp upstream to *F10A3.11* sequence) amplified from
812 genomic DNA was fused to *mec-8* cDNA amplified from a N2 mixed-stage cDNA library and to
813 *SL2::GFP* amplified from pMO46[17] using PCR fusion. *F10A3.11* is predicted by the CenGEN and
814 our dataset to be specific to PLM in hermaphrodites, and in males it is predicted to be expressed
815 in PLM and RIV. Our observations show that its expression is specific in the tail, but it is expressed
816 in 2-3 additional neurons in the head. *capa-1p* (2154 bp upstream to *capa-1* sequence) and

817 *F32B3.5*p (2805 bp upstream to *F32B4.5* sequence) were amplified from genomic DNA and fused
818 to *GFP::H2B* amplified from genomic DNA of *ins-39::GFP::H2B* knock-in animals[31] using PCR
819 fusion. For *dat-1p::novoGFP::cla-1* generation we amplified *dat-1* promoter from a *dat-1p::IRE-1*
820 plasmid[86] and *novoGFP::cla-1* from a plasmid kindly provided by Ithai Rabinowitch and Peri
821 Kurshan.

822 **Touch assays**

823 Gentle touch assays were based on[87]. In brief, L4 animals were isolated the day before the
824 experiment and stored at 20°C overnight. On the day of the experiment, single 1-day adult
825 animals were transferred into NGM plates freshly seeded with 30 µl OP50. After 30 minutes of
826 habituation, animals were tested by applying a touch to the posterior part of the animal
827 (anteriorly to the anus) with an eyelash. Touch was applied when worms were not moving or
828 moved very slowly. Each worm was tested five times with intervals of at least 10 seconds between
829 each trial. The tested worm was given a score of one if it moved forward in response to the touch,
830 and zero if it did not move forward. The response index was then calculated as the average of the
831 forward responses. For anterior gentle touch responses, the anterior part of the animal was
832 touched with an eyelash and a reverse movement response was scored. For harsh tail touch
833 assays, animals were tested by applying a touch to the tail with a flattened platinum wire pick as
834 previously described[88] and their forward movements were scored similarly to animals subjected
835 to posterior gentle touch.

836 **Single Molecule Fluorescent in Situ Hybridization**

837 *mec-8* CAL Fluor Red 590 nm custom probe was designed using Stellaris designer
838 (https://www.biosearchtech.com/stellaris-designer). All the reagents were ordered from

839 Biosearch Technologies and most of the preparations are based on their protocol (Stellaris RNA
840 FISH – protocol for *C. elegans*), with minor adjustments. Synchronized L4 worm population
841 expressing *mec-4p::GFP (zdIs5)* was washed three times with M9 to remove bacterial residues.
842 Then, after aspirating the M9, 1 mL of fixation buffer (4% formaldehyde in 1XPBS) was added to
843 the worms followed by 45 minutes incubation at room temperature. After fixation, worms were
844 washed twice with 1XPBS and supplemented with 70% ethanol. Worms were stored at 4°C
845 overnight. The next day, larvae pellet was centrifuged, and the ethanol was discarded. Worms
846 were then added with 1 mL Wash Buffer A (2 mL Stellaris RNA FISH Wash Buffer A (Biosearch
847 Technologies Cat# SMF-WA1-60), 7 mL Nuclease-free water, 1 mL Deionized Formamide) and
848 incubated at room temperature for 5 minutes. After discarding Wash Buffer A (spin down), worms
849 were dispensed with 100 µL of the Hybridization Buffer containing probe (2 µL of probe set (12.5
850 µM in TE buffer)) into a mixture of 100 µL Hybridization Buffer (450 µL Stellaris RNA FISH
851 Hybridization Buffer, Biosearch Technologies Cat# SMF-HB1-10 and 50 µL Deionized Formamide)
852 to achieve 250 nM probe solution and incubated at 37°C in the dark overnight. In the morning,
853 worms were washed once with Wash Buffer A and incubated with Wash Buffer A at 37°C in the
854 dark for 30 minutes. Then, Wash Buffer A was discarded, and worms were added 1 mL DAPI (4',6-
855 diamidino-2-phenylindole, Wash Buffer A consisting of 5 ng/mL DAPI) to stain the nuclei and
856 incubated at 37°C in the dark for 30 minutes. Then, DAPI was discarded, and worms were added
857 with 1 mL of Wash Buffer B (Biosearch Technologies Cat# SMF-WB1-20) and incubated for 5
858 minutes at room temperature. After discarding Wash Buffer B, 30 µL Vectashield® Mounting
859 Medium (Vector Laboratories Cat #H-1000) were added to the worms for imaging. Imaging was
860 done using Zeiss LSM 880 confocal microscope with 63x oil immersion objective. To image large

861 sample size, we stored samples at 4°C for a few weeks with no signal loss. To differentiate between
862 hermaphrodites and male at all larval stages, we used *ins-39*::SL2::GFP::H2B CRISPR knock-in
863 worms as described previously[31]. For quantification, we followed a protocol based on[89]. We
864 performed Gauss blur filter of sigma = 1 for every image. Then, we performed for each image
865 "Max Entropy" thresholding in Fiji that was selected based on trial-and-error process done on 2-
866 3 representative images. Then, we carried particle analysis for the image in the ROI determined
867 by the GFP channel. This gives a count for the number of particles in a specific ROI. We also
868 performed manual counting of smFISH puncta and got the same results.

869 **Calcium imaging**

870 To image spontaneous calcium traces in PLM, we used animals expressing *mec-4p::GCaMP3.35*.
871 Using a drop of S-basal with 10 mM levamisole that was filtered with 0.22 um filter, adult worms
872 were inserted in a dual olfactory chip that was a kind gift from Michael Krieg lab, fabricated as
873 previously described[90,91]. The flow rate in the chip was 0.005 ml/min. Imaging was done with a
874 Zeiss LSM 880 confocal microscope using a 40x magnification water objective. When the worm
875 was properly located inside the chip, PLM was imaged for 1150 frames (2.8 minutes), with
876 imaging rate of 6.667 Hz. For analysis, the GCaMP fluorescence intensity was measured using FIJI.
877 ROIs of PLM soma were marked manually to extract mean intensity values. Data analysis was
878 performed using Python 3.12. For each worm, the baseline fluorescent level (F0) was calculated
879 by averaging the mean values of 100 frames in the beginning of each recording. Then, for each
880 frame, ΔF was calculated by subtracting F0 from the value of that time point, and the result was
881 divided by F0, to normalize the differences in the fluorescence baseline levels between individuals
882 (ΔF/F0). To calculate the differences between the sexes in PLM basal activity, we performed

883 Fourier transform on the ΔF/F0 values, then the amplitudes were normalized for each worm to
884 its own maximum value. Finally, AUC (area under the curve) was measured using the trapz
885 function in Python, using frequencies up to 2 Hz.

886 **RNAi-Induced Gene Silencing**

887 Gene silencing using RNA interference was carried out as described previously using the feeding
888 protocol on agar plates[92]. Hermaphrodites at L4 stage were fed on HT115 bacteria expressing
889 dsRNA (source Ahringer library) for the targeted genes or on control bacteria harboring empty
890 RNAi vector, L4440. Posterior (gentle) touch responses at 1-day adult from their progeny were
891 scored. The RNAi efficiency was measured using *pos-1* RNAi as a positive control. For every RNAi
892 experiment, a new *pos-1* control was prepared.

893 **Optogenetic stimulation assay**

894 To measure the response of mechanosensory stimulus to the head and tail of hermaphrodite and
895 male *C. elegans* worms, we used AML470[93] strain that expresses light-gated ion channel Chrimson
896 and a fluorescent reporter mCherry in all the six gentle touch neurons under the control of *mec-4*
897 promoter. L4 males and hermaphrodites were isolated a day prior to the day of experiments. Males
898 were separated from hermaphrodites to make sure that they are not mated. The worms were
899 transferred to freshly seeded plates consisting of 1 ml of 0.5 mM all-trans-retinal (Sigma-Aldrich Cat.
900 # R2500) mixed with *E. Coli* (OP50) as food source and stored in the dark at 20°C until the next day.
901 Day 1 adult male and hermaphrodite worms were used in the optogenetic behavior assay. On the
902 day of experiment 20-30 worms were transferred to the unseeded agarose plates to carry out
903 behavior assay while delivering optogenetic stimulation. To measure the response of
904 mechanosensory stimulus to head and tail of male and hermaphrodites, we delivered optogenetic

905 stimulus to the worms using a high throughput optogenetic delivery system[93,94]. Optogenetic
906 stimulation protocol was same as described in the previous work[93]. Briefly, a 400-µm diameter red
907 light stimulation was delivered to either the head, tail, or both simultaneously to each tracked worm
908 on the agarose plate. The illumination spot was centered on the tip of the head or tail of the worm.
909 Optogenetic stimulus of 630 nm wavelength was delivered through a computer-controlled projector
910 for 1 second with an inter trigger stimulus interval of 30 seconds. The stimulus intensity was randomly
911 drawn independently for the head and the tail from the set of 0 and 80 $\mu W/mm^2$ intensities. Thus,
912 there were four stimulus combinations: 1) Head: 0 $\mu W/mm^2$, Tail 0 $\mu W/mm^2$ 2) Head: 0 $\mu W/mm^2$,
913 Tail 80 $\mu W/mm^2$, 3) Head: 80 $\mu W/mm^2$, Tail 0 $\mu W/mm^2$, and 4) Head: 80 $\mu W/mm^2$, Tail 80 $\mu W/mm^2$.
914 Each behavior assay lasted for 30 minutes. The analysis of camera frames of the behavior assay was
915 same as described in the previous studies[93,94]. Briefly, two independent sets of behavior mapping
916 algorithms were employed, one for real-time tracking of worms and optogenetic stimulus delivery,
917 and the other for post processing analysis. The real-time algorithm in LabVIEW tracked all the worms
918 on the agarose plate and calculated various behavior parameters of each worm such as velocity, body
919 curvature, centerline, etc. The first and last index of the centerline were assigned as head and tail
920 respectively. Every 30 seconds, the real-time algorithm signals the computer-controlled projector to
921 deliver optogenetic stimulus to the head, tail, or both simultaneously for every tracked worm with
922 one of the four stimulus intensity combinations. In the post-processing algorithm, we correct for any
923 error in the assignment of head and tail of the worm. This algorithm also classifies behavior of the
924 worm by classifying pose dynamics into a behavior map of forward, reverse, and turns[94,95]. Same
925 analysis steps were used as in the previous study to determine the change in velocity[93]. The velocity
926 of the worm two seconds prior to stimulus onset was defined as the initial velocity of the worm. The

927 velocity of the worm at the end of one second stimulus was defined as the final velocity. Change in
928 velocity for each stimulus event for a worm was defined as the difference between the final velocity
929 and the initial velocity.

930 **Correlation analysis**

931 The entire analysis was done using Python 3.12. Using the number of outgoing connections
932 calculated for Figure 4 (See Supplementary Table 5), we generated for each sex a matrix including
933 the number of outgoing connections and mean expression values of all genes taken from
934 Supplementary Tables 6-7 across the 62 sex-shared neuronal clusters (Supplementary Table 4).
935 Genes that were not expressed in any of the 62 clusters were removed from the analysis. Then, we
936 performed Pearson correlation calculation with Benjamini-Hochberg False Discovery Rate (FDR)
937 correction for each comparison to account for multiple comparisons, providing correlation coefficient
938 for each gene in the data set of hermaphrodites and male separately. We refer in the text to
939 significantly correlated genes to genes with p-valued adjusted < 0.05.

940 **Quantification and statistical analysis**

941 Each figure legend and relevant method section include information regarding quantification,
942 statistical testing, and sample size.

943 **Data availability**

944 All data generated or analyzed in this manuscript are provided in the supplementary information
945 files. The Supplementary Table 2,6,7 contains the RNA-seq datasets related to this article. The
946 sequence data of this article have been submitted to NCBI and are available under BioProject
947 XXXX.

948 **ACKNOWLEDGEMENTS**

949 We thank members of the Oren-Suissa lab and Laurent lab for their critical insights regarding the
950 manuscript. We thank Dr. Joseph Dicken and Dr. Efrat Hagai at Flow Cytometry Unit, Life Science
951 Core Facility, Weizmann Institute of Science for helping with FACS sorting. scRNA-seq library
952 preparation was done with critical advice from Dr. Hadas Keren-Shaul, Dr. Merav Kedmi and Dr.
953 David Pilzer from the Genomics Sandbox unit at the Life Science Core Facility of Weizmann
954 Institute of Science. We thank Sapir Sela from the Oren-Suissa lab for cloning the *dat-*
955 *1p::novogfp::cla-1* plasmid. We are grateful to Oliver Hobert lab for sharing strains. Some strains
956 used in this study were obtained from *Caenorhabditis* Genetics Center (CGC), which is funded by
957 the NIH Office of Research Infrastructure Programs (P40 OD010440). We thank WormAtlas which
958 is supported by NIH OD 010943. We are thankful to Alon Zaslaver, Ithai Rabinowitch, Peri Kurshan,
959 Hannes Buelow labs for providing plasmids. We thank Michael Krieg lab for providing the dual-
960 olfactory chips. We thank WormBase, an online biological database for *C. elegans*, which is
961 supported by Grant U41 HG002223 from the National Human Genome Research Institute at the
962 NIH, the UK Medical Research Council, and the UK Biotechnology and Biological Sciences
963 Research Council. MOS acknowledges financial support from the European Research Council ERC-
964 2019-STG 850784, Israel Science Foundation grant 961/21, Dr. Barry Sherman Institute for
965 Medicinal Chemistry, Sagol Weizmann-MIT Bridge Program and the Azrieli Foundation. MOS is
966 the incumbent of the Jenna and Julia Birnbach Family Career Development Chair. MOS and PL are
967 supported by HORIZON TMA MSCA Doctoral Networks grant # 101119745.

968 **AUTHOR CONTRIBUTIONS**

969 R.H. conducted and generated scRNA-seq data and carried out NeuroPAL imaging and analysis.
970 R.L. and P.L. performed the scRNA-seq data analysis; assigned neuron identities; analyzed

971 expression. G.S. helped with scRNA-seq initial datasets generation. RR helped with thresholding.
972 H.S. performed the ranking analysis, neurotransmitter identity with correlation analysis, the
973 functional analysis of PLM, AVG and PHC neurons including imaging gene expression, calcium
974 imaging and behavioral experiments and the correlation analysis and imaging presented in Figure
975 7. G.G. and E.S. contributed to the conceptualization and performance of correlation analysis. Y.S.
976 generated and conducted *capa-1* reporter expression. S.N.H. contributed to the *lad-2* mutant
977 experiments. S.K. performed and analyzed the optogenetic experiments A.L. supervised the
978 optogenetic experiments. M.O.S. supervised and designed the experiments. R.H., H.S., R.L., P.L.
979 and M.O.S. wrote the paper.

980 **DECLARATION OF INTERESTS**

981 The authors declare no competing interests.

982 **RESOURCE AVAILABILITY**

983 **Lead Contact**

984 Further information and requests for resources and reagents should be directed to and will be
985 fulfilled by the Lead Contact, Meital Oren-Suissa (meital.oren@weizmann.ac.il).

986 **Material Availability**

987 Unique strains generated in this study have been deposited at the *Caenorhabditis* Genetics
988 Center. Requests for other strains and plasmids should be directed to the Lead Contact.

989 **REFERENCES**

990 1. Gater, R. *et al.* Sex differences in the prevalence and detection of depressive and anxiety
991 disorders in general health care settings: report from the World Health Organization
992 Collaborative Study on Psychological Problems in General Health Care. *Arch Gen*
993 *Psychiatry* **55**, 405–413 (1998).

2. Cerri, S., Mus, L. & Blandini, F. Parkinson's Disease in Women and Men: What's the Difference? *J Parkinsons Dis* **9**, 501–515 (2019).
3. Aleman, A., Kahn, R. S. & Selten, J. P. Sex differences in the risk of schizophrenia: evidence from meta-analysis. *Arch Gen Psychiatry* **60**, 565–571 (2003).
4. Fang, S. *et al.* Sexually dimorphic control of affective state processing and empathic behaviors. *Neuron* **112**, 1498-1517.e8 (2024).
5. Chiu, H. *et al.* Erratum: A circuit logic for sexually shared and dimorphic aggressive behaviors in Drosophila (Cell (2021) 184(2) (507–520.e16), (S0092867420316202), (10.1016/j.cell.2020.11.048)). *Cell* **184**, 847 (2021).
6. Pechuk, V. *et al.* Reprogramming the topology of the nociceptive circuit in C. elegans reshapes sexual behavior. *Current Biology* **32**, 4372-4385.e7 (2022).
7. Setty, H. *et al.* Sexually dimorphic architecture and function of a mechanosensory circuit in C. elegans. *Nat Commun* **13**, (2022).
8. Moffitt, J. R. *et al.* Molecular, spatial, and functional single-cell profiling of the hypothalamic preoptic region. *Science* **362**, (2018).
9. Chen, P. B. *et al.* Sexually Dimorphic Control of Parenting Behavior by the Medial Amygdala. *Cell* **176**, 1206-1221.e18 (2019).
10. Welch, J. D. *et al.* Single-Cell Multi-omic Integration Compares and Contrasts Features of Brain Cell Identity. *Cell* **177**, 1873-1887.e17 (2019).
11. Kim, D. W. *et al.* Multimodal Analysis of Cell Types in a Hypothalamic Node Controlling Social Behavior. *Cell* **179**, 713-728.e17 (2019).
12. Gegenhuber, B., Wu, M. V., Bronstein, R. & Tollkuhn, J. Gene regulation by gonadal hormone receptors underlies brain sex differences. *Nature 2022 606:7912* **606**, 153–159 (2022).
13. Knoedler, J. R. *et al.* A functional cellular framework for sex and estrous cycle-dependent gene expression and behavior. *Cell* **185**, 654-671.e22 (2022).
14. Li, F. *et al.* Sex differences orchestrated by androgens at single-cell resolution. *Nature 2024 629:8010* **629**, 193–200 (2024).
15. Zarkower, D. Somatic sex determination. *WormBook* 1–12 (2006) doi:10.1895/WORMBOOK.1.84.1.
16. Barr, M. M., García, L. R. & Portman, D. S. Sexual Dimorphism and Sex Differences in Caenorhabditis elegans Neuronal Development and Behavior. *Genetics* **208**, 909–935 (2018).
17. Oren-Suissa, M., Bayer, E. A. & Hobert, O. Sex-specific pruning of neuronal synapses in Caenorhabditis elegans. *Nature* **533**, 206–211 (2016).
18. Fagan, K. A. *et al.* A Single-Neuron Chemosensory Switch Determines the Valence of a Sexually Dimorphic Sensory Behavior. *Current Biology* **28**, 902-914.e5 (2018).
19. Lawson, H. N., Wexler, L. R., Wnuk, H. K. & Portman, D. S. Dynamic, Non-binary Specification of Sexual State in the C. elegans Nervous System. *Curr Biol* **30**, 3617-3623.e3 (2020).
20. Taylor, S. R. *et al.* Molecular topography of an entire nervous system. *Cell* **184**, 4329-4347.e23 (2021).
21. Roux, A. E. *et al.* Individual cell types in C. elegans age differently and activate distinct cell-protective responses. *Cell Rep* **42**, 112902 (2023).

1038 22. Ghaddar, A. *et al.* Whole-body gene expression atlas of an adult metazoan. *Sci Adv* **9**,
1039 eadg0506 (2023).
1040 23. Ma, F. & Zheng, C. Transcriptome age of individual cell types in Caenorhabditis elegans.
1041 *Proc Natl Acad Sci U S A* **120**, e2216351120 (2023).
1042 24. Lorenzo, R., Onizuka, M., Defrance, M. & Laurent, P. Combining single-cell RNA-
1043 sequencing with a molecular atlas unveils new markers for Caenorhabditis elegans
1044 neuron classes. *Nucleic Acids Res* **48**, 7119–7134 (2020).
1045 25. Truong, L. *et al.* Single-nucleus resolution mapping of the adult C. elegans and its
1046 application to elucidate inter- and trans-generational response to alcohol. *Cell Rep* **42**,
1047 (2023).
1048 26. Packer, J. S. *et al.* A lineage-resolved molecular atlas of C. elegans embryogenesis at
1049 single-cell resolution. *Science* **365**, (2019).
1050 27. Cao, J. *et al.* Comprehensive single-cell transcriptional profiling of a multicellular
1051 organism. *Science* **357**, 661–667 (2017).
1052 28. Hashimshony, T., Wagner, F., Sher, N. & Yanai, I. CEL-Seq: Single-Cell RNA-Seq by
1053 Multiplexed Linear Amplification. *Cell Rep* **2**, 666–673 (2012).
1054 29. Schumacher, B., Gallrein, C. & Meyer, D. Neuron-type specific aging-rate reveals age
1055 decelerating interventions preventing neurodegeneration. (2024) doi:10.21203/RS.3.RS-
1056 4360587/V1.
1057 30. Purice, M. D. *et al.* Molecular heterogeneity of C. elegans glia across sexes. *bioRxiv* (2023)
1058 doi:10.1101/2023.03.21.533668.
1059 31. Haque, R. *et al.* Sex-specific developmental gene expression atlas unveils dimorphic gene
1060 networks in C. elegans. *Nature Communications 2024 15:1* **15**, 1–18 (2024).
1061 32. Pereira, L. *et al.* Timing mechanism of sexually dimorphic nervous system differentiation.
1062 *Elife* **8**, (2019).
1063 33. Pereira, L. *et al.* A cellular and regulatory map of the cholinergic nervous system of C.
1064 elegans. *Elife* **4**, (2015).
1065 34. Serrano-Saiz, E., Oren-Suissa, M., Bayer, E. A. & Hobert, O. Sexually Dimorphic
1066 Differentiation of a C. elegans Hub Neuron Is Cell Autonomously Controlled by a
1067 Conserved Transcription Factor. *Current Biology* **27**, 199–209 (2017).
1068 35. Cook, S. J. *et al.* Whole-animal connectomes of both Caenorhabditis elegans sexes.
1069 *Nature* **571**, 63–71 (2019).
1070 36. Hunter, C. P. & Wood, W. B. The tra-1 gene determines sexual phenotype cell-
1071 autonomously in C. elegans. *Cell* **63**, 1193–1204 (1990).
1072 37. Berkseth, M., Ikegami, K., Arur, S., Lieb, J. D. & Zarkower, D. TRA-1 ChIP-seq reèeals
1073 regulators of sexual differentiation and multileèel feedback in nematode sex
1074 determination. *Proc Natl Acad Sci U S A* **110**, 16033–16038 (2013).
1075 38. Yemini, E. *et al.* NeuroPAL: A Multicolor Atlas for Whole-Brain Neuronal Identification in
1076 C. elegans. *Cell* **184**, 272-288.e11 (2021).
1077 39. Tekieli, T. *et al.* Visualizing the organization and differentiation of the male-specific
1078 nervous system of C. elegans. *Development* **148**, (2021).
1079 40. Mclntire, S. L., Jorgensen, E. & Horvitz, H. R. Genes required for GABA function in
1080 Caenorhabditis elegans. *Nature 1993 364:6435* **364**, 334–337 (1993).

1081 41. Sulston, J., Dew, M. & Brenner, S. Dopaminergic neurons in the nematode Caenorhabditis
1082 elegans. *Journal of Comparative Neurology* **163**, 215–226 (1975).
1083 42. Wang, C. *et al.* A neurotransmitter atlas of the nervous system of C. elegans males and
1084 hermaphrodites. *Elife* **13**, (2024).
1085 43. Hobert, O. Terminal Selectors of Neuronal Identity. *Curr Top Dev Biol* **116**, 455–475
1086 (2016).
1087 44. Chalfie, M. & Sulston, J. Developmental genetics of the mechanosensory neurons of
1088 Caenorhabditis elegans. *Dev Biol* **82**, 358–370 (1981).
1089 45. Chalfie, M. & Sulston, J. Developmental genetics of the mechanosensory neurons of
1090 Caenorhabditis elegans. *Dev Biol* **82**, 358–370 (1981).
1091 46. Chen, X. & Chalfie, M. Regulation of Mechanosensation in C. elegans through
1092 Ubiquitination of the MEC-4 Mechanotransduction Channel. *The Journal of Neuroscience*
1093 **35**, 2200 (2015).
1094 47. O'Hagan, R., Chalfie, M. & Goodman, M. B. The MEC-4 DEG/ENaC channel of
1095 Caenorhabditis elegans touch receptor neurons transduces mechanical signals. *Nature*
1096 *Neuroscience 2004 8:1* **8**, 43–50 (2004).
1097 48. Stober, W., Fink, A., Bohn, E., Chalfie, M. & Au, M. Genetic control of differentiation of the
1098 caenorhabditis elegans touch receptor neurons. *Science (1979)* **243**, 1027–1033 (1989).
1099 49. Wang, X. *et al.* The C. elegans L1CAM homologue LAD-2 functions as a coreceptor in
1100 MAB-20/Sema2–mediated axon guidance. *J Cell Biol* **180**, 233 (2008).
1101 50. Arnatkevičiūtė, A., Fulcher, B. D., Pocock, R. & Fornito, A. Hub connectivity, neuronal
1102 diversity, and gene expression in the Caenorhabditis elegans connectome. *PLoS Comput*
1103 *Biol* **14**, e1005989 (2018).
1104 51. Baruch, L., Itzkovitz, S., Golan-Mashiach, M., Shapiro, E. & Segal, E. Using Expression
1105 Profiles of Caenorhabditis elegans Neurons To Identify Genes That Mediate Synaptic
1106 Connectivity. *PLoS Comput Biol* **4**, e1000120 (2008).
1107 52. Nonet, M. L. Visualization of synaptic specializations in live C. elegans with synaptic
1108 vesicle protein-GFP fusions. *J Neurosci Methods* **89**, 33–40 (1999).
1109 53. Xuan, Z. *et al.* Clarinet (CLA-1), a novel active zone protein required for synaptic vesicle
1110 clustering and release. *Elife* **6**, (2017).
1111 54. Zhen, M. & Jin, Y. The liprin protein SYD-2 regulates the differentiation of presynaptic
1112 termini in C. elegans. *Nature 1999 401:6751* **401**, 371–375 (1999).
1113 55. McDonald, N. A., Tao, L., Dong, M. Q. & Shen, K. SAD-1 kinase controls presynaptic phase
1114 separation by relieving SYD-2/Liprin-α autoinhibition. *PLoS Biol* **21**, e3002421 (2023).
1115 56. Putrenko, I., Zakikhani, M. & Dent, J. A. A Family of Acetylcholine-gated Chloride Channel
1116 Subunits in Caenorhabditis elegans. *Journal of Biological Chemistry* **280**, 6392–6398
1117 (2005).
1118 57. Steger, K. A. & Avery, L. The GAR-3 Muscarinic Receptor Cooperates With Calcium Signals
1119 to Regulate Muscle Contraction in the Caenorhabditis elegans Pharynx. *Genetics* **167**,
1120 633–643 (2004).
1121 58. Tanizawa, Y. *et al.* Inositol monophosphatase regulates localization of synaptic
1122 components and behavior in the mature nervous system of C. elegans. *Genes Dev* **20**,
1123 3296 (2006).

59. Bénard, C., Tjoe, N., Boulin, T., Recio, J. & Hobert, O. The Small, Secreted Immunoglobulin Protein ZIG-3 Maintains Axon Position in Caenorhabditis elegans. *Genetics* **183**, 917 (2009).
60. Aurelio, O., Hall, D. H. & Hobert, O. Immunoglobulin-domain proteins required for maintenance of ventral nerve cord organization. *Science (1979)* **295**, 686–690 (2002).
61. Serrano-Saiz, E. *et al.* A Neurotransmitter Atlas of the Caenorhabditis elegans Male Nervous System Reveals Sexually Dimorphic Neurotransmitter Usage. *Genetics* **206**, 1251–1269 (2017).
62. Hammarlund, M., Hobert, O., Miller, D. M. & Sestan, N. The CeNGEN Project: The Complete Gene Expression Map of an Entire Nervous System. *Neuron* **99**, 430–433 (2018).
63. Qian, T., Wang, H., Xia, X. & Li, Y. Current and emerging methods for probing neuropeptide transmission. *Curr Opin Neurobiol* **81**, 102751 (2023).
64. Ripoll-Sánchez, L. *et al.* The neuropeptidergic connectome of C. elegans. *Neuron* **111**, 3570-3589.e5 (2023).
65. Peedikayil-Kurien, S., Haque, R., Gat, A. & Oren-Suissa, M. Modulation by NPYR underlies experience-dependent, sexually dimorphic learning. *bioRxiv* 2023.10.19.563073 (2023) doi:10.1101/2023.10.19.563073.
66. Susoy, V. *et al.* Natural sensory context drives diverse brain-wide activity during C. elegans mating. *Cell* **184**, 5122-5137.e17 (2021).
67. Lipton, J., Kleemann, G., Ghosh, R., Lints, R. & Emmons, S. W. Mate Searching in Caenorhabditis elegans: A Genetic Model for Sex Drive in a Simple Invertebrate. *Journal of Neuroscience* **24**, 7427–7434 (2004).
68. Liu, T., Kim, K., Li, C. & Barr, M. M. FMRFamide-like neuropeptides and mechanosensory touch receptor neurons regulate male sexual turning behavior in Caenorhabditis elegans. *J Neurosci* **27**, 7174–7182 (2007).
69. Wang, X. *et al.* The C. elegans L1CAM homologue LAD-2 functions as a coreceptor in MAB-20/Sema2–mediated axon guidance. *J Cell Biol* **180**, 233 (2008).
70. Brenner, S. THE GENETICS OF CAENORHABDITIS ELEGANS. *Genetics* **77**, 71–94 (1974).
71. Zhang, S., Banerjee, D. & Kuhn, J. R. Isolation and Culture of Larval Cells from C. elegans. *PLoS One* **6**, e19505 (2011).
72. Spencer, W. C. *et al.* Isolation of Specific Neurons from C. elegans Larvae for Gene Expression Profiling. *PLoS One* **9**, e112102 (2014).
73. Kaletsky, R. *et al.* The C. elegans adult neuronal IIS/FOXO transcriptome reveals adult phenotype regulators. *Nature 2015 529:7584* **529**, 92–96 (2015).
74. Katz, M. *et al.* Glutamate spillover in C. elegans triggers repetitive behavior through presynaptic activation of MGL-2/mGluR5. *Nature Communications 2019 10:1* **10**, 1–13 (2019).
75. Young, M. D. & Behjati, S. SoupX removes ambient RNA contamination from droplet-based single-cell RNA sequencing data. *Gigascience* **9**, 1–10 (2020).
76. Bhattacharya, A., Aghayeva, U., Berghoff, E. G. & Hobert, O. Plasticity of the Electrical Connectome of C. elegans. *Cell* **176**, 1174-1189.e16 (2019).
77. Stefanakis, N., Carrera, I. & Hobert, O. Regulatory Logic of Pan-Neuronal Gene Expression in C. elegans. *Neuron* **87**, 733–750 (2015).

78. Reilly, M. B., Cros, C., Varol, E., Yemini, E. & Hobert, O. Unique homeobox codes delineate all the neuron classes of C. elegans. *Nature 2020 584:7822* **584**, 595–601 (2020).
79. Harris, T. W. *et al.* WormBase: a modern Model Organism Information Resource. *Nucleic Acids Res* **48**, D762–D767 (2020).
80. Davison, A. C. & Hinkley, D. V. Bootstrap Methods and their Application. *Bootstrap Methods and their Application* (1997) doi:10.1017/CBO9780511802843.
81. Canty, A. & Ripley, B. D. boot: Bootstrap R (S-Plus) Functions. Preprint at (2024).
82. Davison, A. C. & Hinkley, D. V. Bootstrap Methods and their Application. *Bootstrap Methods and their Application* (1997) doi:10.1017/CBO9780511802843.
83. Schindelin, J. *et al.* Fiji: an open-source platform for biological-image analysis. *Nat Methods* **9**, 676–682 (2012).
84. Holdorf, A. D. *et al.* WormCat: An Online Tool for Annotation and Visualization of Caenorhabditis elegans Genome-Scale Data. *Genetics* **214**, 279–294 (2020).
85. Hobert, O. PCR fusion-based approach to create reporter Gene constructs for expression analysis in transgenic C. elegans. *Biotechniques* **32**, 728–730 (2002).
86. Levi-Ferber, M. *et al.* Neuronal regulated ire- 1-dependent mRNA decay controls germline differentiation in Caenorhabditis elegans. *Elife* **10**, (2021).
87. Chalfie, M., Hart, A. C., Rankin, C. H. & Goodman, M. B. Assaying mechanosensation. *WormBook* (2014) doi:10.1895/WORMBOOK.1.172.1.
88. Li, W., Kang, L., Piggott, B. J., Feng, Z. & Xu, X. Z. S. The neural circuits and sensory channels mediating harsh touch sensation in Caenorhabditis elegans. *Nature Communications 2011 2:1* **2**, 1–9 (2011).
89. Ji, N. & van Oudenaarden, A. Single molecule fluorescent in situ hybridization (smFISH) of C. elegans worms and embryos. *WormBook* 1–16 (2012) doi:10.1895/WORMBOOK.1.153.1.
90. Karimi, S., Gat, A., Agazzi, C., Oren-Suissa, M. & Krieg, M. Automated dual olfactory device for studying head/tail chemosensation in Caenorhabditis elegans. *APL Bioeng* **8**, (2024).
91. Gat, A. *et al.* Integration of spatially opposing cues by a single interneuron guides decision-making in C. elegans. *Cell Rep* **42**, (2023).
92. Ahringer, J. Reverse genetics. *WormBook* (2006) doi:10.1895/WORMBOOK.1.47.1.
93. Liu, M., Kumar, S., Sharma, A. K. & Leifer, A. M. A high-throughput method to deliver targeted optogenetic stimulation to moving C. elegans populations. *PLoS Biol* **20**, e3001524 (2022).
94. Kumar, S., Sharma, A. K., Tran, A., Liu, M. & Leifer, A. M. Inhibitory feedback from the motor circuit gates mechanosensory processing in Caenorhabditis elegans. *PLoS Biol* **21**, e3002280 (2023).
95. Liu, M., Sharma, A. K., Shaevitz, J. W. & Leifer, A. M. Temporal processing and context dependency in caenorhabditis elegans response to mechanosensation. *Elife* **7**, (2018).